



Dynamic simulation of building VAV air-conditioning system and evaluation of EMCS on-line control strategies

Shengwei Wang*

Department of Building Services Engineering, The Hong Kong Polytechnic University, Kowloon, Hong Kong

Received 28 November 1997; accepted 21 September 1998

Abstract

Dynamic models are developed to simulate the thermal, hydraulic, environmental and mechanic characteristics and energy performance of a building and VAV air-conditioning system under the control of EMCS. Three on-line supervisory strategies and programs based on integrated EMCS stations are developed to optimise the VAV static pressure set-point, AHU outlet air temperature set-point and outdoor ventilation air flow set-point. The strategies and programs are commissioned and evaluated under the simulated 'real-life' environment. This paper presents the dynamic models, the control strategies and the simulation exercises for commissioning and evaluation of the strategies. © 1999 Elsevier Science Ltd. All rights reserved.

Nomenclature

A	area (m^2)	amb	ambient
C	CO_2 concentration (ppm)	CAV	CAV
c, c_p	specific heat, specific heat of air (kJ/kg K)	exf	exfiltration
$C2$	pollutant concentration (ppm)	exh	exhaust
CS	strength of CO_2 source ($10^{-6}m^3/s$)	fh	outdoor air
DP	differential pressure (Pa)	fut	furniture
G	humidity (kg/kg)	inf	infiltration
GS	strength of humidity source (kg/s)	leak	leakage
H	damper position (0–1)	out	outside
h	convection coefficient (kW/m^2K)	P	occupants
L	distance (m)	R	room (or space)
M	mass of air (kg)	rtn	return air
m	mass flow rate (kg/s)	s	supply air
N	number of occupants	SA	'sol-air'
P	pressure (Pa)	VAV	VAV
PS	strength of pollutant source ($10^{-6}m^3/s$)	wi	wall inside
Q	heat load (kW)	win	window
R	heat resistance (K/kW)	zone	occupied zone
T	temperature (K)		
u	velocity (m/s)		
V	volume (m^3)		
v	volume flow rate (m^3/s)		
ρ_a	specific mass of air (kg/m^3)		

Subscripts and superscripts

abs absorbed

*Tel.: 00852 27665859; fax: 00852 27746146; e-mail: beswwang@polyu.edu.hk

1. Introduction

Dynamic simulation of HVAC system provides a convenient and low cost tool in testing, commissioning and evaluating HVAC system control strategies or the control programs implemented in Energy Management and Control Systems (EMCS) [1, 2]. Dynamic models, which are convenient to use and well represent the dynamic characteristics in all the aspects of concern, are the basis for practical applications.

Recently, many researchers have focused on dynamic

modelling and simulation of HVAC systems. Studies on the VAV air-conditioning system dynamic modelling and simulation for control applications are also being conducted. A transient model of a two zone VAV (variable air volume) is developed by Zaheer-Uddin and Zhen [3]. The building and VAV air-conditioning system is simulated by House and Smith as a test facility for studying the optimal control [4]. The programs such as TRNSYS, DOE-2, HVACSIM⁺, etc., also provide models to simulate VAV air-conditioning systems [5–7]. Two VAV system dynamic simulation packages were developed in the framework of emulation exercises within IEA (BCS) Annex 17 to evaluate the control strategies in real EMCS [1]. However, those models focus on simulating the thermal dynamic and energy characteristics.

When the on-line control performance of supervisory and local control strategies are of concern in order to test, evaluate and commission the strategies under simulated 'real-life' conditions, the realistic characteristics of air flow-pressure balance needs to be incorporated into the system simulation. The real-life environmental behaviour of the system also needs to be incorporated into the system simulation due to the increasing concern on the effects of control strategies on indoor environment. This was not sufficiently addressed in the past although there are studies [8] conducted to study the environmental control strategies using simulation method. The simulation test of on-line supervisory strategies implemented in integrated digital stations of EMCS also requires the simulation of the integrated VAV system of large scale.

In this study, dynamic models of building and VAV air-conditioning systems, which incorporate the thermal, hydraulic, environmental (i.e. CO₂ and pollutant) and mechanic characteristics and energy performance, are developed to simulate the system controlled by strategies implemented in EMCS using a model-based program.

On-line control strategies for optimising the VAV static pressure set-point, AHU (air handling unit) outlet air temperature set-point and the outdoor ventilation air flow set-point are developed. The VAV static pressure set-point optimisation strategy minimises the pressure set-point while sufficient air flow to individual VAV terminals is provided. The temperature optimisation strategy resets the temperature set-point to ensure that insufficient ventilation in individual zone is avoided whilst the effects on energy and space temperature control are incorporated. The outdoor air ventilation flow set-point supervisory strategy consists in a demanded ventilation control strategy according to the revised ASHRAE standard 62-1989R [9] supported by a dynamic occupancy detection approach based on CO₂ measurement and an enthalpy control strategy.

The realistic models of VAV system local DDC controls and the supervisory control strategies implemented in the integrated digital stations of EMCS are developed and incorporated into the VAV system simulation. Two

simulation exercises were conducted. In the first exercise, the programs and strategies are commissioned and tuned. The second exercise is an exercise to test and evaluate on-line performance of the control strategies. The strategies were evaluated under four different weather conditions selected from different seasons in Hong Kong.

2. Building and VAV system

The building is a forty-six storey commercial building located in Hong Kong. The floor under study is an open plan office of about 2300 square meters usable floor area. Two central air handling units (AHU) serve the floor. Each serves half of the floor. One AHU consists of a VAV system and a CAV system. There are forty VAV dampers and over a hundred air diffusers associated with one AHU. The design air flow rates of the VAV system and CAV system are 6 m³/s and 1.4 m³/s, respectively. The design VAV supply fan pressure at the location of pressure sensor is 650 Pa.

One AHU/VAV system and their associated buildings are simulated to test the control, energy performances and indoor air quality of the VAV system under the control of on-line optimal strategies implemented in EMCS. The office simulated has a floor area of 1166 m². It is air-conditioned using VAV and CAV systems. The perimeter zones orientating north are equipped with CAV terminals beside VAV terminals, and the others are equipped with VAV terminals only.

The floor area is divided into eight zones when simulating the office floor. Six of the zones are perimeter zones and the other two are interior zones. The area and air volume of the zones are shown in Fig. 1. A schematic of the air-conditioning system serving the office floor is presented in Fig. 2. The chilled water flow rates of the cooling coils are moderated to control the coil outlet air temperature. Two variable blade angle fans are equipped as VAV supply fan and return fan, respectively. The CAV supply fan is a constant fan. The pitch angle of the VAV supply (axial) fan is moderated to control the supply air static pressure. The return (axial) fan is controlled to control the exfiltration flow rate in order to maintain positive pressure in the building. It is achieved by controlling the difference between the total supply and return air flow rates within the upper and lower limits by moderating the pitch angle of the return fan.

3. System component models

3.1. Simplified building model

A simplified building model simulates the dynamic balance of energy, moisture, CO₂ and a pollutant, which is suitable for testing the control, energy and environmental performances of on-line local and supervisory control

North

	145m ²	175m ²	175m ²	145m ²
West	566m ³	683m ³	663m ³	566m ³
	110m ²	153m ²	153m ²	110m ²
	429m ³	597m ³	597m ³	429m ³
East				

Fig. 1. Selection of zones of simulated floor.

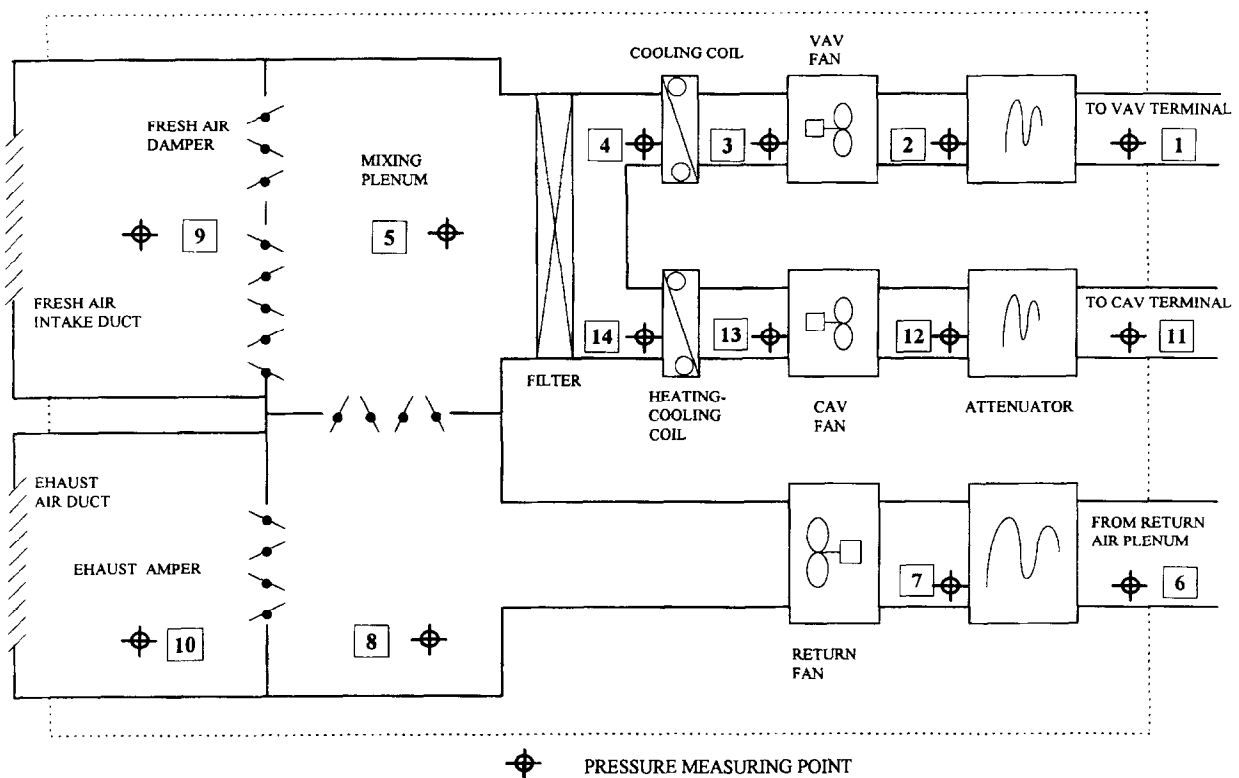


Fig. 2. Schematic of Air Handling Unit (AHU) and pressure measurement points.

strategies. It is developed on the basis of the concept of the building model developed in the IEA Annex 10 and 17 [10, 11]. The modelling of CO₂ and another pollutant aims at simulating the occupant and non-occupant generated pollutants although both can be used to simulate

any type of pollutants if the relevant generation sources are properly modified.

The model represents the open plan office floor by a network of thermal resistance, thermal capacitance and air volume. Figure 3 illustrates the principle of the

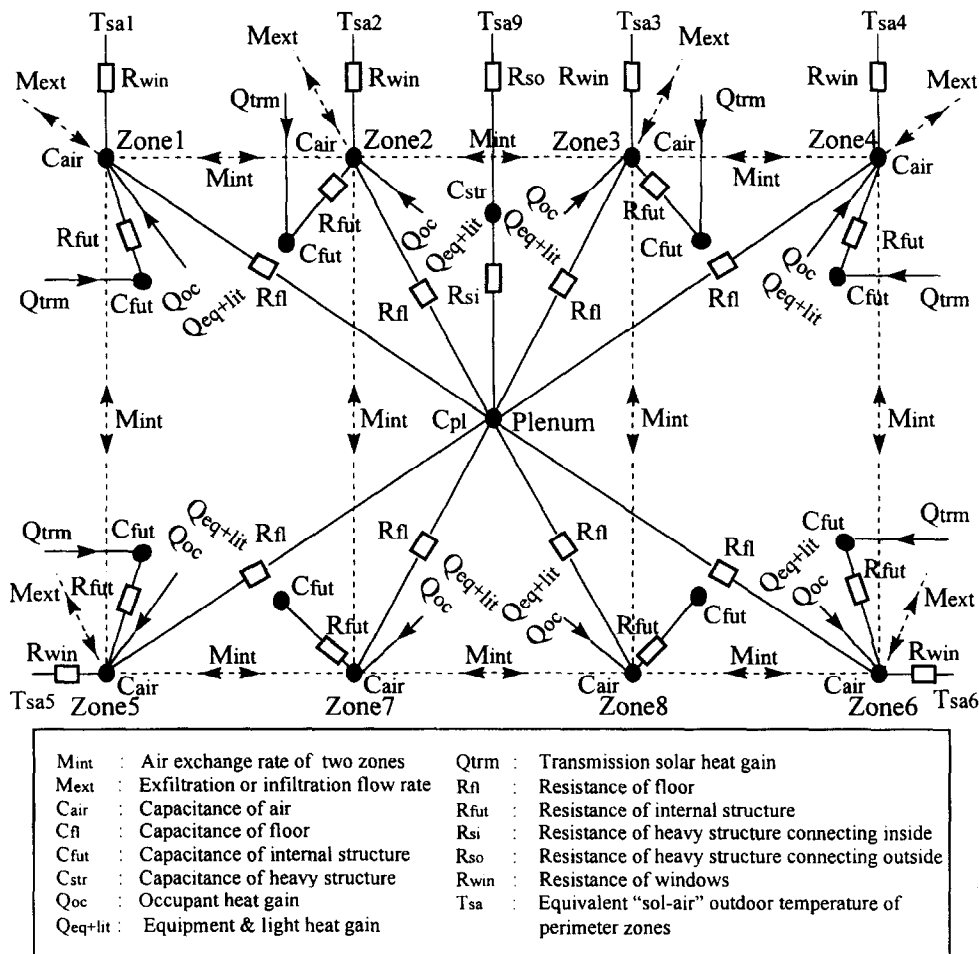


Fig. 3. Illustration of building thermal model.

dynamic energy balance of the open plan office divided with the multiple spaces or air volumes. Each space is considered as a node of well mixed air volume with uniform temperature, moisture, CO₂ and pollutant concentration. The connections between zones are the air mass exchanges caused by air flow. The external wall of each zone is represented by a node of thermal capacitance and resistance linking the zone with outside. The external walls of a zone are categorised to be heavy wall and light wall. An external wall is considered to be a heavy wall when the thermal capacitance is relatively large and affects the heat transfer to the zone significantly. On the contrary, it is considered to be a light wall. The thermal capacitance of heavy external walls is represented by a thermal capacitance, while the thermal capacitance of light external walls is neglected and only their resistance is considered. The internal structure and furniture in each zone are represented by a node of thermal capacitance connected to the zone through a thermal resistance.

The model uses a simplified method to compute the heat load of solar radiation absorbed by the external

walls by means of an equivalent 'sol-air' temperature. The 'sol-air' temperature is defined here as an equivalent temperature, which takes account of the effect of the solar radiation absorbed by building external walls (including absorbency and emission) as the effect of increment of outside air temperature to building. The solar heat gain transmitted through the windows is added directly to the node of the internal structure and furniture of a relevant zone. It is firstly absorbed by internal structures and furniture, and then released to the zone air due to the temperature difference. It is modified from the conventional definition of the 'sol-air' temperature [10], which is used in the building model of IEA Annex 10 and 17.

Each zone node employs four ordinary differential equations describing the balance of energy, moisture, CO₂ and non-occupant generated pollutant. The dynamic balances of an occupied zone i ($i = 1, 2, \dots, 8$) are shown in eqns (1)–(4). Since the occupied zones fully use double layer glass as external walls with relatively low thermal capacitance, only the resistance is considered in the model

and the thermal capacitance is neglected. The external wall of the plenum employed concrete structure. Both thermal capacitance and resistance are considered.

$$M_i c_p \frac{dT_i}{dt} = Q_i + m_{VAV,i} c_p (T_{VAV} - T_i) + m_{CAV,i} c_p (T_{CAV} - T_i) + m_{inf,i} c_p (T_{amb} - T_i) - m_{exf,i} c_p T_i + \sum_j m_{ij} c_p (T_j - T_i) + \frac{T_{w,i} - T_i}{R_{wi,i}} + \frac{T_{fut,i} - T_i}{R_{fut,i}} + \frac{T_{sa,i} - T_i}{R_{win,i}} \quad (1)$$

$$M_i \frac{dG_i}{dt} = GS_i + m_{VAV,i} (G_{VAV} - G_i) + m_{CAV,i} (G_{CAV} - G_i) + m_{inf,i} (G_{amb} - G_i) - m_{exf,i} G_i + \sum_j m_{ij} (G_j - G_i) \quad (2)$$

$$V_i \frac{dC_i}{dt} = CS_i + v_{VAV,i} (C_{VAV} - C_i) + v_{CAV,i} (C_{CAV} - C_i) + v_{inf,i} (C_{amb} - C_i) - v_{exf,i} C_i + \sum_j v_{ij} (C_j - C_i) \quad (3)$$

$$V_i \frac{dC2_i}{dt} = PS_i + v_{VAV,i} (C2_{VAV} - C2_i) + v_{CAV,i} (C2_{CAV} - C2_i) + v_{inf,i} (C2_{amb} - C2_i) - v_{exf,i} C2_i + \sum_j v_{ij} (C2_j - C2_i) \quad (4)$$

Where, T , G , C and $C2$ are the space air temperature, humidity, CO_2 and pollutant concentrations, respectively. Q , GS , CS and PS are the total internal heat, moisture, CO_2 and pollutant generation rates, respectively, in a zone. M and V are the total air mass and volume, respectively, in a zone. m and v are the mass and volume flow rates. R_{wi} is the thermal resistance of external wall node in connection to the indoor air node of a zone. R_{fut} is the thermal resistance of internal structure and furniture node in connection to indoor air node of a zone. R_{win} is the thermal resistance of indoor air node in connection to outside. The values of infiltration and exfiltration flow rates are positive only and they cannot have nonzero values in the same time.

The equivalent 'sol-air' temperature of a zone is defined as the equilibrium temperature of the zone internal node when the solar radiation absorbed by building external walls is the only heat sources of the zone (i.e. internal heat load and other external heat load are zero) and when the zone is isolated from other zones. The equivalent 'sol-air' temperature of a zone (T_{SA}) can be calculated by summarising the equivalent 'sol-air' temperatures of all the external walls of the zone using equation (5). The equivalent 'sol-air' temperature of an external wall ($T_{SA,i}$) is defined in equation (6).

$$T_{SA} = \frac{\sum_{i=1}^m \frac{T_{SA,i}}{R_i}}{\sum_{i=1}^m \frac{1}{R_i} + C_{inf}} \quad (5)$$

$$T_{SA,i} = T_{out} + \frac{1}{A_i h_{out,i}} Q_{abs} \quad (6)$$

Where, R_i is the overall heat transfer resistance of an external wall, A_i is the area of a wall, $h_{out,i}$ is the convection coefficient of a wall on the external surface, Q_{abs} is the rate of heat absorbed by an external wall. C_{inf} is the capacity flow rate of infiltration air to the zone.

The air exchange rate between zones, m_{ij} (or v_{ij}) is affected by the velocity of the supply air, the difference between the air temperatures in the zones, the size of the zone and other factors (such as the effect of walking of occupancy). In this building model, a mean air velocity of each zone is introduced to evaluate air exchange rate [12, 13]. The air mass exchange rate between any other neighbour is computed using eqn (7). The mean air velocity (u_{ij}) consists of two parts: one ($u_{1,i}$ and $u_{1,j}$) considering the effects of the supply air flow rate and another ($u_{2,ij}$) considering the effects of the natural convection caused by the temperature difference.

$$m_{ij} = \rho_a A_{ij} u_{ij} = \rho_a A_{ij} \left(\frac{u_{1,i} + u_{1,j}}{2} + u_{2,ij} \right) \quad (7)$$

$$u_{1,i} = \frac{m_{sup,i} L_i}{M_i} \quad (8)$$

$$u_{2,ij} = \xi \sqrt{\frac{2|T_i - T_j|}{T_i + T_j}} \quad (9)$$

Where, L is the distance between the outlet of supply air and the inlet of return air, M_i is the air mass of a zone, $M_{sup,i}$ is total supply air mass flow rate of A/C system to the zone, T_i and T_j are the air temperature of the zones, ρ_a is the air density, and ξ is a coefficient depending on the geometry of a zone [14].

3.2. System pressure-flow balance

A model is developed to simulate the pressure-flow balance of the building and air-conditioning system. The model is illustrated in Fig. 4. The effects of air velocity and wind effect on the system pressure-flow balance is neglected.

The flow resistances of the VAV and CAV filters and cooling coils are considered to be constant. The constant flow resistance before VAV pressure sensor represents the resistance of the air attenuator and duct before the sensor. The resistance of the air duct after the VAV pressure sensor is considered to be constant. The constant CAV duct flow resistance represents the flow resistance of the CAV air attenuator and duct. The flow resistances of the CAV terminals and diffusers are considered to be constant. The resistances of VAV terminals and diffusers are variables, which depend on the positions of the VAV dampers. The pressure in the entire occupied space is considered to be uniform when simulating the system

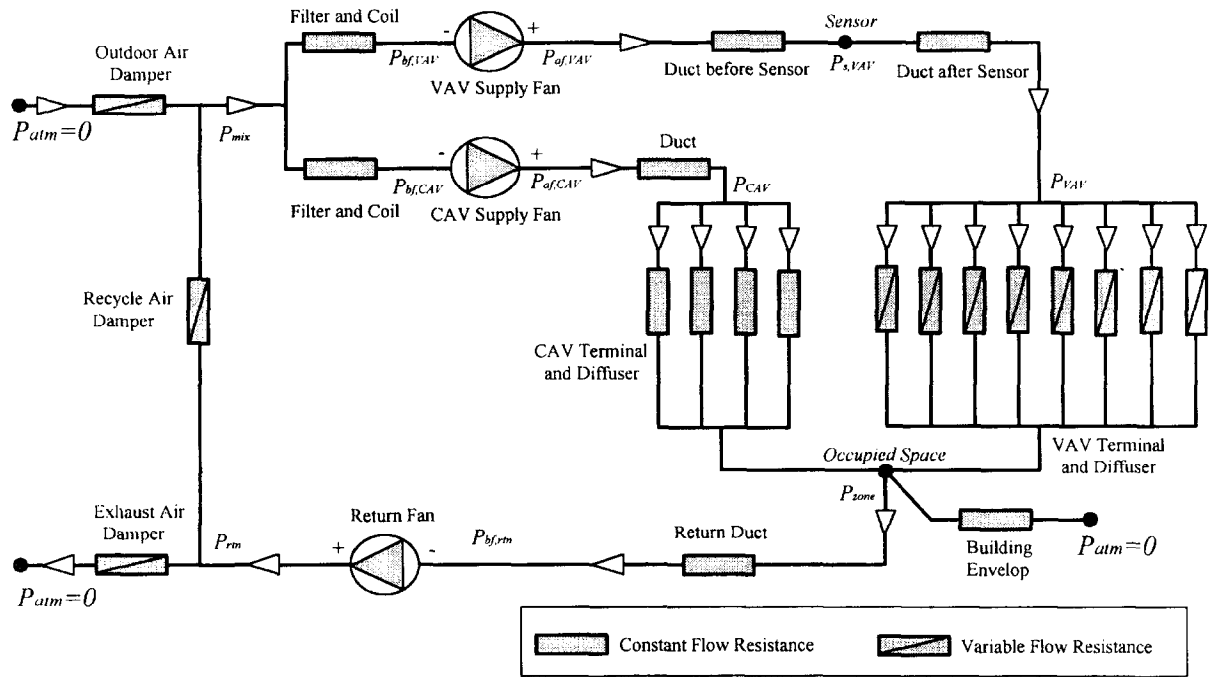


Fig. 4. Schematic of system pressure-flow balance model.

pressure-flow balance. The air leakage through the building envelop is computed by assuming a constant flow resistance linking the occupied space to outside. The flow resistance of return duct is considered to be constant. The resistances of the outdoor air, recycle air and exhaust air dampers vary according to the positions of the dampers.

The static pressure-flow characteristics of the VAV supply fan, CAV supply fan and return fan are simulated by separate models. The pressure flow balance computation is based on the air mass conservation and pressure balance. The air mass balance of the system is shown in eqns (10)–(12). The pressure balance of the system is shown in eqn (13)–(15). The pressure drop on each flow resistance (i.e. component) is represented by eqn (16).

$$m_{sup} = m_{sup,VAV} + m_{sup,CAV} = \sum_{i=1}^8 m_{VAV,i} + \sum_{i=1}^4 m_{CAV,i} \quad (10)$$

$$m_{rtn} = m_{sup} - m_{exf} \quad (11)$$

$$m_{rec} = m_{rtn} - m_{exh} = m_{sup} - m_{out} \quad (12)$$

$$DP_{fan,VAV} - DP_{fc,VAV} - DP_{d,bsl} - DP_{d,asl} - DP_{VAV} = P_{zone} - P_{mix} \quad (13)$$

$$DP_{fan,CAV} - DP_{fc,CAV} - DP_{d,CAV} - DP_{CAV} = P_{zone} - P_{mix} \quad (14)$$

$$DP_{fan,rtn} - DP_{d,rtn} - DP_{rec} = P_{mix} - P_{zone} \quad (15)$$

$$DP_i = R_i \cdot |v_i| \cdot v_i \quad (16)$$

Tests show that serious convergence difficulty exists in

the iteration process when simulating the air system living pressure-flow balance by adding the component flow characteristics directly into the corresponding thermal performance models using the component based simulation programs designed for building thermal performance simulation. Therefore, one single component model is used in the study to simulate the system pressure-flow balance in order to avoid the problems of convergence. The iteration process of the system pressure-flow balance controlled by DDC is illustrated in Fig. 5.

Providing the resistance of the system components, duct, damper and the delivery static pressure head of three fans, the system pressure-flow balance model computes the flow rates and pressure at different locations of the system. When simulating the pressure-flow balance at each simulation step, iteration of three fan delivery pressure heads and air flow rate through the fans takes place until they are converged. The damper models and control models are not involved in the iteration of system pressure-flow balance computation at a simulation step. The controllers will update the control according to the change of the controlled pressure and flow rates. These control actions will change the fan curve due to the change of pitch angle and the resistances of the relevant dampers. But these changes affect the pressure-flow balance of following steps only and do not affect the iteration process of the current simulation step. The fan characteristics and damper resistance are unchanged during the iteration when simulating the pressure-flow balance at a simulation step.

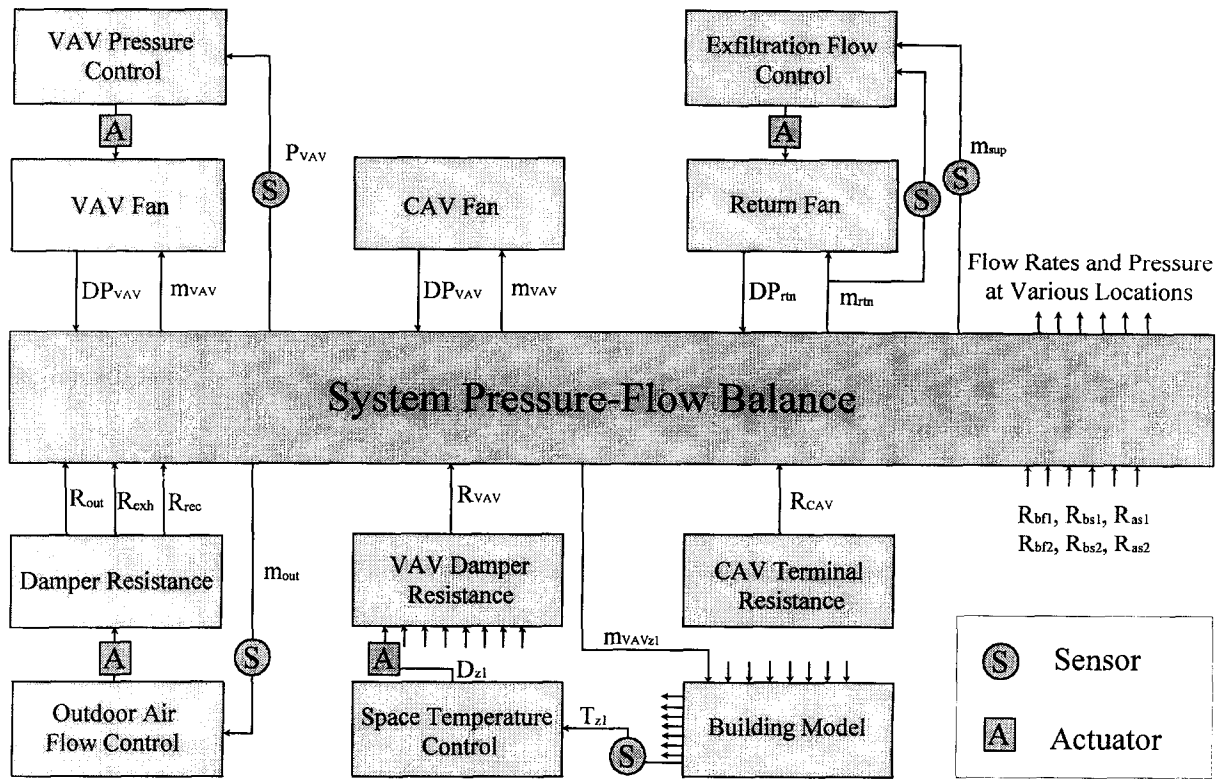


Fig. 5. Illustration of iteration process for system pressure-flow balance simulation.

The flow resistance of an individual damper at certain damper position (H) is calculated using Legg's exponential correlation [15]. The air flow (v_{nom}) passing through a damper at nominal pressure head is calculated using eqns (17) and (18) for damper with opposed blades and parallel blades, respectively. The flow resistance (R) is then calculated according to eqn (19).

$$v_{nom} = (1 - H) \cdot v_{leak} + H \cdot e^{4.725 \cdot (H-1)} \quad (17)$$

$$v_{nom} = (1 - H) \cdot v_{leak} + H \cdot e^{3.789 \cdot (H-1)} \quad (18)$$

$$R = \frac{R_{min}}{v_{nom}^2} \quad (19)$$

3.3. Duct model

A duct model is developed to simulate the heat loss through duct wall, dynamic effects of the duct wall and the effects of transfer delay on temperature, moisture, CO₂ and the pollutant. A duct is divided into a number of sections considering the duct length and the velocity range of the air flowing inside. The process of the air flowing in the duct at a simulation step is assumed consisting of three separate 'sub-processes': moving of the air segments; mixing of air within individual sections and the heat exchange with outside through duct wall.

The air segments are assumed to reach their end pos-

itions of the step within infinitesimal time. After the air segments have reached their end positions of the step, the air within one duct section is mixed within infinitesimal time. The new temperature, moisture content CO₂ and pollutant concentrations within each duct section are computed assuming perfect mixing. A dynamic heat exchange process then takes place between the air with each section and the environment through the wall of relevant sections. This heat exchange process wholly occupies the time of a simulation step. The new air segments transferring in the next simulation step is the air volume within individual zone sections after the heat exchange process. The heat exchange of the duct wall along the air flow direction is neglected.

The duct outlet temperature, moisture content, CO₂ and pollutant concentrations are that of the well mixed air volume of the air segments leaving the duct at a simulation step. The heat exchange process is illustrated in Fig. 6. The heat exchange of an air segment between two simulation steps is represented by two differential equations as follows. The initial air temperature of a section is the temperature of the well mixed air in the section. The initial duct temperature of a section is the duct temperature at the end of heat exchange in the previous step.

$$C_{a,i} \frac{dT_{a,i}}{dt} = \frac{T_{w,i} - T_{a,i}}{R_{1,i}} \quad (20)$$

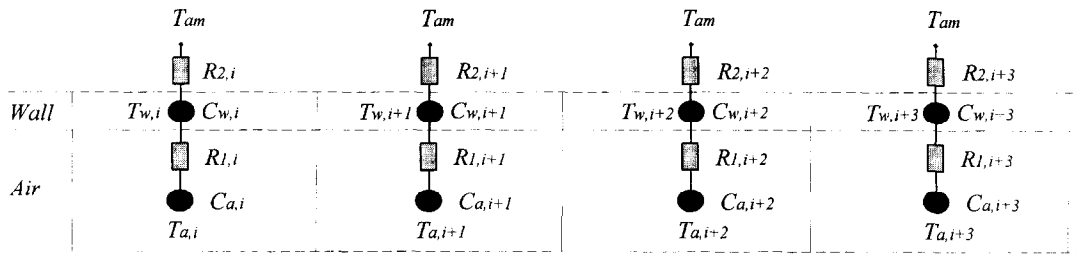


Fig. 6. Schematic of duct thermal model.

$$C_{w,i} \frac{dT_{w,i}}{dt} = \frac{T_{a,i} - T_{w,i}}{R_{1,i}} + \frac{T_{am} - T_{w,i}}{R_{2,i}} \quad (21)$$

3.4. Fan models

To simulate an axial fan, the state of the fan is represented by three normalised variables (φ , ξ , λ) [16] representing the air volume flow rate, fan total pressure rise and fan absorbed power, respectively, as shown in eqns (22)–(24).

$$\varphi = \frac{4 \cdot v_a}{\pi^2 \cdot D^3 \cdot N} \quad (22)$$

$$\xi = \frac{2 \cdot PT_{fan}}{\rho_a \cdot (\pi \cdot D \cdot N)^2} \quad (23)$$

$$\lambda = \frac{800 \cdot W_{fan}}{\pi^4 \cdot D^5 \cdot N^3 \cdot \rho_a} \quad (24)$$

The fan performance law is fitted by a polynomial of two-variables of normalised air flow rate (φ) and fan pitch angle (θ) as eqns (25) and (26). The steady-state pressure rise of the fan is obtained from the fan total pressure rise using eqn (27). The fan motor power input (W_{mot}), using eqn (28), is obtained from the fan absorbed power (W_{fan}) and the efficiencies of the fan and motor (η_{fan} , η_{mot}), which are affected by the fan power.

$$\xi = \sum_{i=0}^{n_1} \left(\sum_{j=0}^{m_1} C_1(i,j) \cdot \varphi^i \cdot \theta^j \right) \quad (25)$$

$$\lambda = \sum_{i=0}^{n_2} \left(\sum_{j=0}^{m_2} C_2(i,j) \cdot \varphi^i \cdot \theta^j \right) \quad (26)$$

$$DP_{fan} = PT_{fan} - P_{nom} \cdot \left(\frac{v_{air}}{v_{nom}} \right)^2 \quad (27)$$

$$W_{mot} = \frac{W_{fan}}{\eta_{fan} \cdot \eta_{mot}} \quad (28)$$

3.5. Cooling coil

A dynamic model is developed to simulate the cooling coil, which is the same model used in the study presented in refs [2, 17]. The model includes a steady-state approach

and a dynamic approach. A first order differential equation is used to represent the dynamics of a coil with lumped thermal mass. The dynamic equation on the basis of energy balance ensures that the energy is conserved.

$$C_c \frac{dt_c}{d\tau} = \frac{t_{a,in} - t_c}{R_1} - \frac{t_c - t_{w,in}}{R_2} \quad (29)$$

Where, t_c is the mean temperature of coil, $t_{a,in}$ and $t_{w,in}$ are the inlet air and water temperatures. C_c is the overall thermal capacity of the coil, R_1 and R_2 are the overall heat transfer resistances at the air and water sides.

The air and water temperatures at the outlet ($t_{a,ex}$, $t_{w,ex}$) therefore can be computed by the heat balances of both sides:

$$t_{a,ex} = t_{a,in} - \frac{SHR(t_{a,in} - t_c)}{R_1 C_a} \quad (30)$$

$$t_{w,ex} = t_{w,in} - \frac{t_c - t_{w,in}}{R_2 C_w} \quad (31)$$

Where, C_a and C_w are the capacity flow rates of air and water, SHR is the sensible heat ratio. SHR uses the same value calculated in the same inlet condition in the steady-state case using the by-pass factor method.

The heat transfer calculation applies the classical Number of Transfer Unit (NTU) and heat transfer effectiveness methods. The classical method to calculate the effect of the fin on air side thermal resistance is applied. Two different methods are used to calculate the heat convection coefficient on air side in dry and wet regions, respectively.

In dry regime, the overall heat transfer resistance (R) is computed as follows. Where, A is the total heat transfer surface area, R_a , R_m and R_w are the heat transfer resistances of air side convection, coil metal and water side convection, N_{row} is the number of row.

$$NTU = \frac{UA}{C_{min}} = \frac{A}{C_{min}(R_a + R_m + R_w)} \quad (32)$$

$$\varepsilon = f\left(N_{row}, \frac{C_{min}}{C_{max}}, NTU\right) \quad (33)$$

$$R = \frac{T_{a,in} - T_{w,in}}{Q} = \frac{1}{\varepsilon \cdot C_{min}} \quad (34)$$

In wet regime, a fictitious air flow is assumed, which has a specific heat equal to the average saturation specific heat (c_s , specific heat of saturation moisture air at the average temperature of air inlet wet bulb temperature and water inlet temperature). The air capacity flow rate and air convection coefficient of the fictitious air flow (C_{af} , $h_{a,wt}$) are as follows. Where, C_{pi} is the specific heat of moisture air.

$$C_{af} = m_a c_s \quad (35)$$

$$h_{a,wt} = h_a \cdot \frac{c_s}{c_{pi}} \quad (36)$$

Then, the overall heat transfer resistance (R) is computed using the same approach. Where, subscript 'wt' represents wet regime, 'f' represents fictitious air flow.

$$NTU_f = \frac{AU}{c_{minf}} = \frac{A}{C_{minf}(R_{a,wt} + R_m + R_w)} \quad (37)$$

$$\varepsilon_f = f\left(N_{row}, \frac{C_{minf}}{C_{maxf}}, NTU_f\right) \quad (38)$$

$$Q_{wt} = \varepsilon_f \cdot C_{minf} \cdot (T_{a,wt} - T_{w,in}) \quad (39)$$

$$\varepsilon_{wt} = \frac{Q_{wt}}{(T_{a,in} - T_{w,in}) \cdot C_{minf}} \quad (40)$$

$$R = \frac{T_{a,in} - T_{w,in}}{Q_{wt}} = \frac{1}{\varepsilon_f \cdot C_{minf}} \quad (41)$$

3.6. DDC controller, sensor and actuator models

A 'realistic' controller model is developed to simulate the DDC controllers [18]. The model represents the following functions of the EMCS: DDC (Direct Digital Control) functions, discrete-time operation of digital controllers and supervisory control strategies.

The time scheduling of a sampling cycle is considered to be four steps: process variable sampling, control outputs computation, control signal output, and waiting time for the next sampling cycle. The PID control function used in DDC loops uses the ISA algorithm. Its discrete form is used in the models.

The actuator model is used to represent the characteristics of actuators [19]. The actuator is assumed to accelerate very quickly and then turn at constant speed. A minimum change (e.g. the sensitivity of the actuator defined as a parameter of the model) in demanded position is required to restart the actuator. The model includes the hysteresis in the linkage between actuators and valves or dampers. If a valve stem is driven by a rotary actuator, the speed of the valve stem varies with the position of the crank.

The dynamics sensor model is used to simulate the temperature, pressure, flow and CO₂ sensors using the time constant method. Different time constants are used

for different sensors depending on the characteristics of the sensors and the measured variables and the locations of the sensors.

4. VAV system performance monitoring

The parameters of VAV models to be used for simulation may be determined according to the VAV component characteristics given in manufacturer catalogues and/or determined according to empirical correlations given in handbooks using the system geometry configuration parameters. In this study, the VAV system performance data needed for determining the parameters of the VAV component models were obtained by monitoring the VAV system on site.

The supply flow rate, return flow rate, and fresh air flow rate and the pressure drops across the dampers, filter, coil, air ducts and VAV dampers are measured under various flow rates by manually changing the supply and return fan pitch angle. The flow resistance of VAV dampers at damper fully open position and minimum position was tested by manually setting the existing controllers. The flow resistance of a damper at fully open position was determined using second order curve fitting. The fan performance curves from manufacturer's catalogues were used to determine the parameters of the fan model.

Figure 7 shows the flow-pressure characteristics, when all the VAV dampers are fully open, and the pressure drop on a VAV damper (including diffusers) at two different positions (fully open and minimum) at different total VAV supply flow rates while the other VAV dampers are fully open. It can be seen that the main proportion of the pressure drop was on the damper. When the damper position changes, the pressure drop changes significantly. Figures 8 and 9 show the flow-pressure characteristics of VAV supply air ductwork and return air ductwork.

Figures 10 and 11 show the flow-pressure characteristics of VAV and CAV filters and coils. It can be observed that the pressure on the filter contributed the major part. It can be also found by comparing Figs 10 and 11 with Fig. 7 that filters contributed significant proportion to the required fan static pressure rise.

5. VAV system on-line control strategies

5.1. Local DDC controls

Figure 12 illustrates the control of central air handling unit. Two DDC controllers control the air temperatures at the outlet of the VAV and CAV coils by moderating the chilled water flow rate through the coils, respectively. The static pressure controller maintains the static pressure at two-third of the VAV supply duct at its set-point

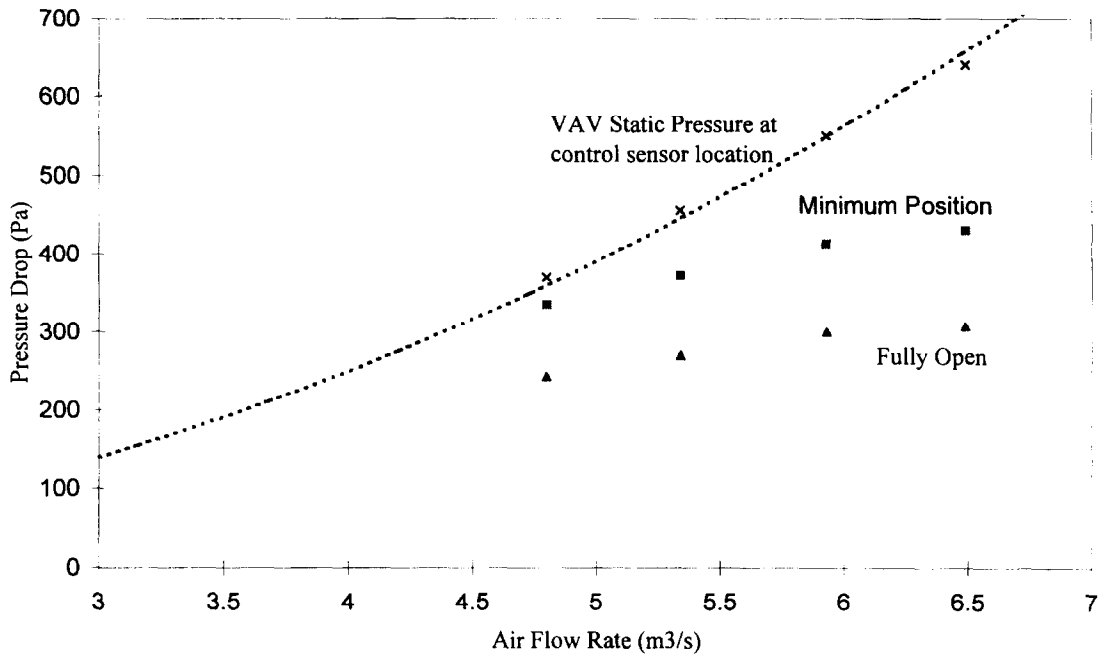


Fig. 7. Pressure drop on VAV damper and diffusers.

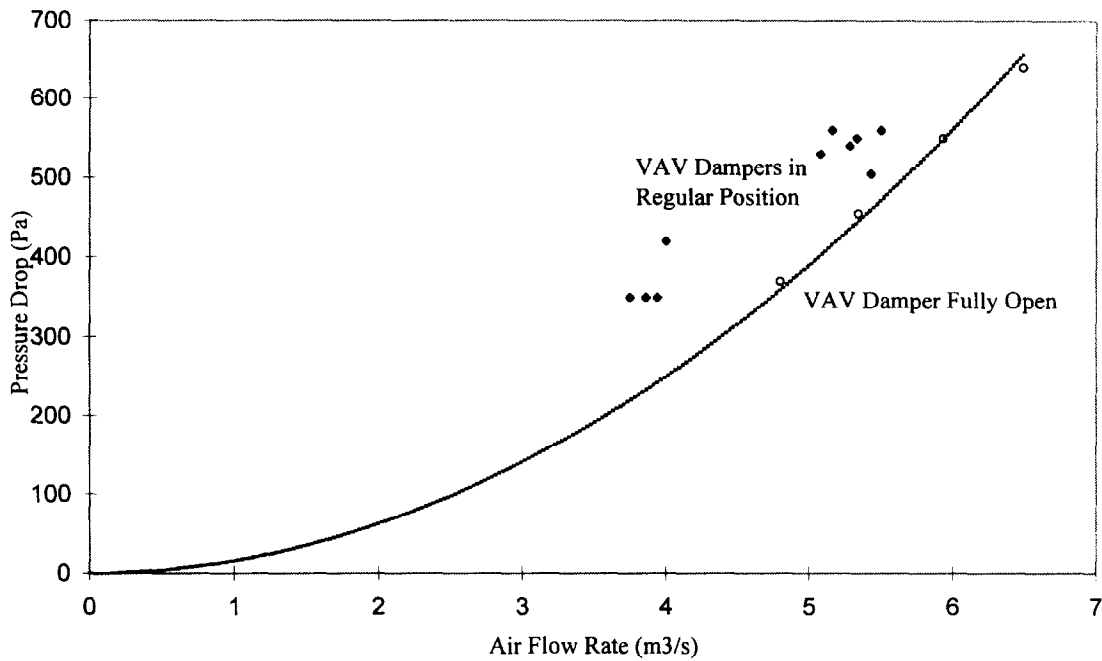


Fig. 8. Overall pressure drop on VAV ductwork and dampers.

by moderating the fan pitch angle of the VAV supply fan. The exfiltration flow controller controls the difference between the total supply and return air flow rates in order to maintain a positive pressure in the building by moderating the pitch angle of the return fan. The outdoor air controller controls the outdoor air flow by moderating the dampers.

The zone space temperature control employs the pressure independent VAV terminal box (Fig. 13). The zone temperature controller maintains the space temperature by regulating the flow set-point. The VAV air flow controller controls the flow rate at its set-point by moderating the VAV damper position. The PID control is used by the local DDC controllers.

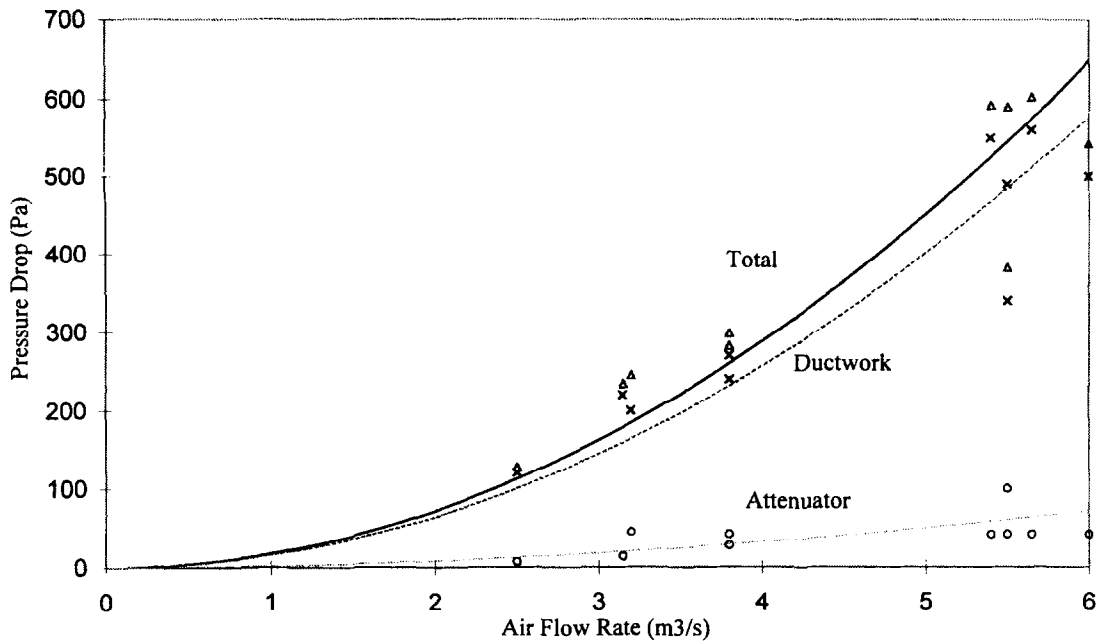


Fig. 9. Pressure-flow characteristics of return ductwork.

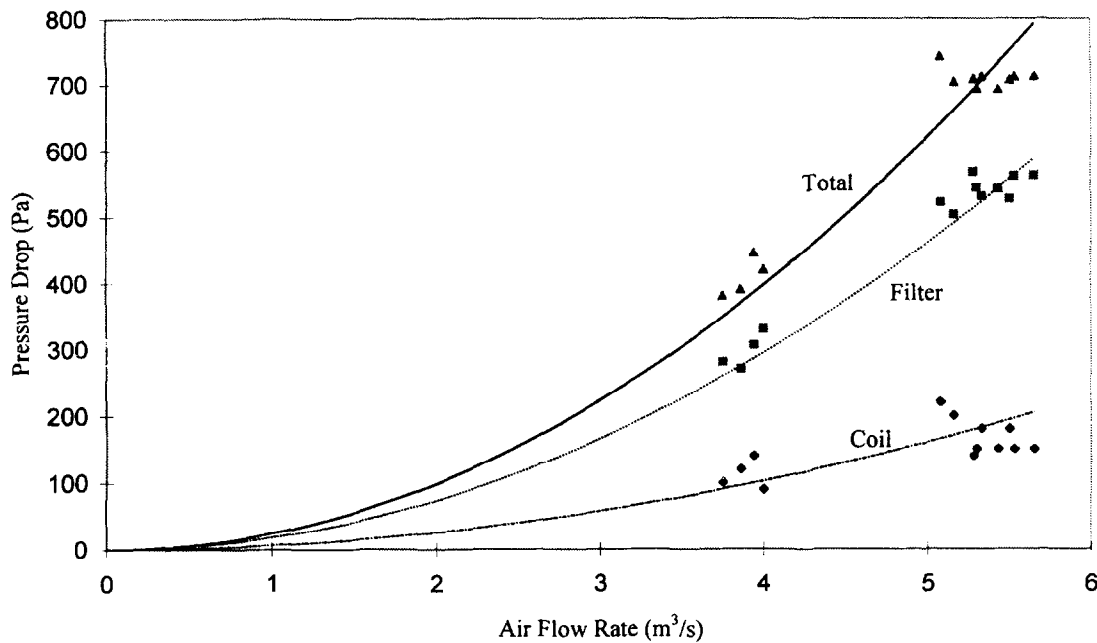


Fig. 10. Pressure-flow characteristics of VAV filter and coil.

5.2. *Optimal outdoor air flow control*

The outdoor air ventilation affects both energy consumption of the VAV system (i.e. coil consumption) and indoor air quality [8, 20]. The change of outdoor air ventilation flow often (but not always) results in two contrary effects on the energy consumption and indoor air quality. The optimisation of outdoor air flow control

is achieved by making a compromise between two control strategies, i.e. combining the enthalpy control and demanded ventilation (Fig. 12).

The outdoor air flow set-point determined by an occupancy-based demanded ventilation control strategy is used to be the low limit for outdoor air control only. The enthalpy control strategy determines an optimal outdoor air flow set-point based on the enthalpy values of outdoor

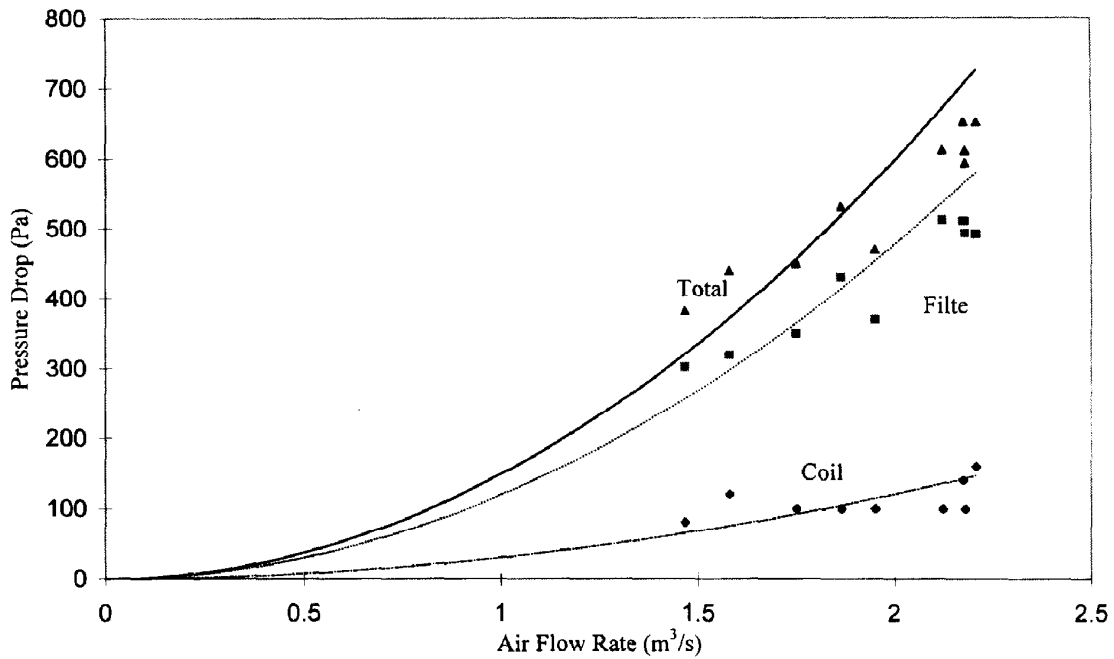


Fig. 11. Pressure-flow characteristics of CAV filter and coil.

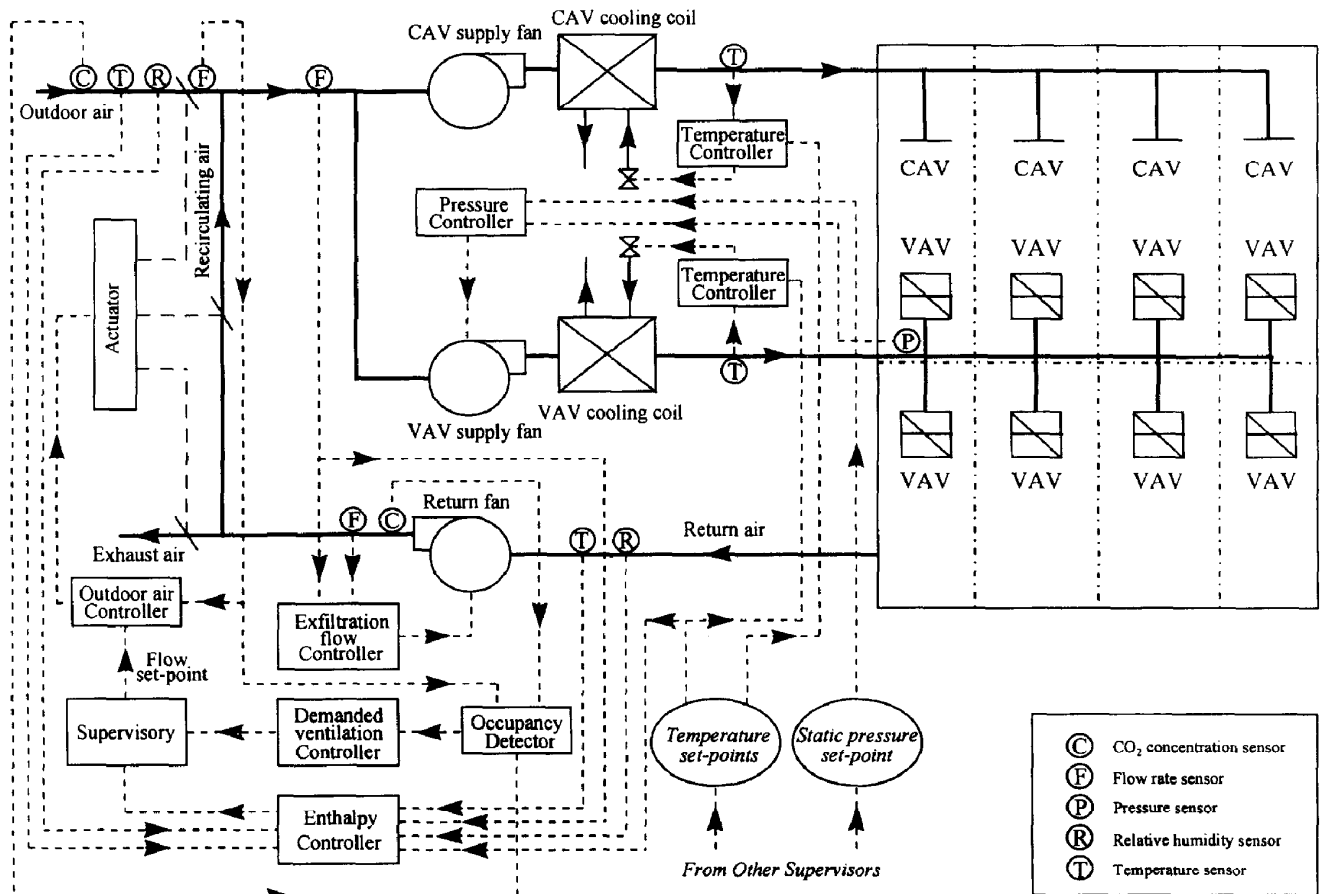


Fig. 12. Local DDC control loops and outdoor air flow supervisory control.

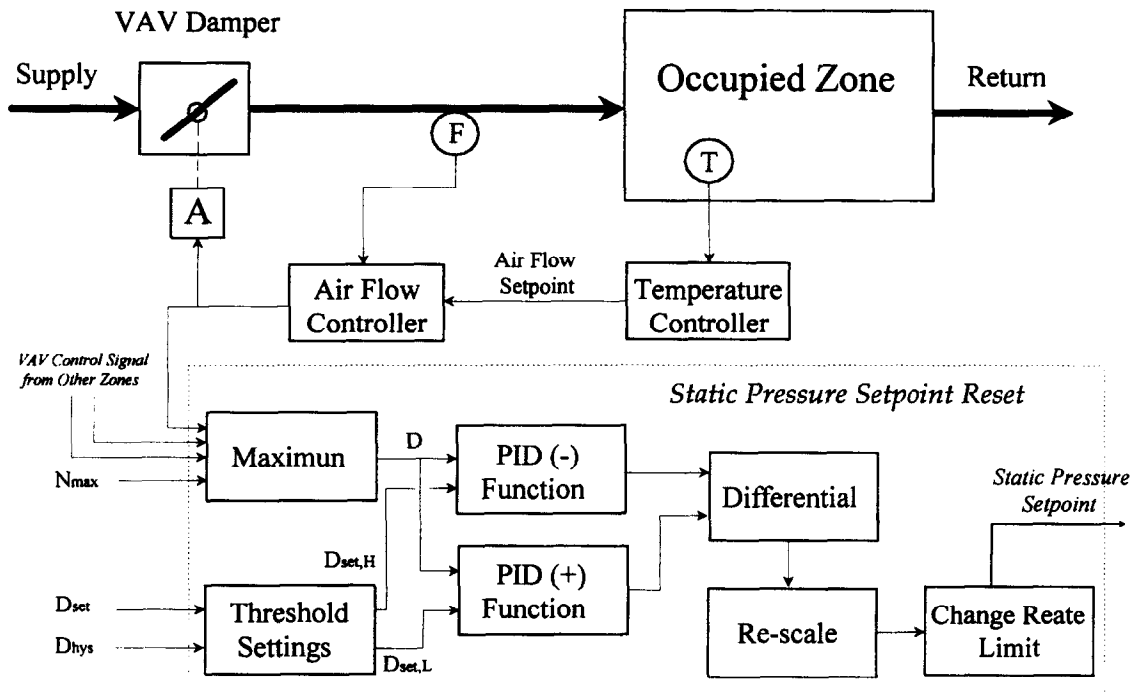


Fig. 13. Schematic of VAV static pressure set-point supervisory strategy.

air and return, total supply air flow rate and AHU supply air temperature set-point. The enthalpy control strategy aims at minimising the coil consumption,

The occupancy-based demanded ventilation is developed to meet the requirement of the new ASHRAE standard 62-1989R [9] on the outdoor air flow. An on-line dynamic strategy is developed to detect the actual occupancy in occupied indoor space. The occupancy detector detects the actual occupancy in the space by sampling CO₂ concentrations of outdoor air and return air. A controller determines the set-point of outdoor air ventilation rate (v_{0A}) on the basis of the new standard 62-1989R, according to eqn (42).

$$v_{0A} = v_p + v_b = R_p N + R_b A \quad (42)$$

Where, v_p is the demanded outdoor air flow concerning occupants and their activity, v_b is that concerning the occupiable area, R_p and R_b are the outdoor air requirements per person and per unit area, respectively, A is the occupiable area and N is the actual space occupancy.

The algorithm of occupancy detector employs a dynamic method as shown in eqn (43) assuming positive pressure in the indoor space. The number of occupancy at current sampling instant can be represented by the CO₂ concentrations and the outdoor air flow rates measured at the current sampling and previous instants as shown in eqn (42). Kalman filter is employed to increase the stability of occupancy detection strategy.

$$N^i = \frac{E_{ac}(v_{th}^i + v_{th}^{i-1})(C_R^i - C_{th}^i)}{2S} + V \frac{C_R^i - C_R^{i-1}}{\Delta t} \quad (43)$$

Where, N is the number of occupants, v_{th} is the outdoor air flow rate, C_R and C_{th} are the CO₂ concentrations of the return air and outdoor air, respectively, V is the total indoor air volume, S is the average CO₂ generation rate per person. Superscript i and $i-1$ represent the current and previous sampling instants, respectively.

5.3. On-line optimal reset of static pressure set-point

This strategy aims at minimising the VAV fan energy consumption by minimising the static pressure [21]. In order to supply sufficient air to every individual zone as well as to minimise the static pressure, the static pressure is controlled to be enough and just enough for the most heavily loaded zones. The on-line strategy makes use of all the VAV damper positions represented by relevant VAV damper position control demands as the indicator of relative load of the individual VAV terminals associated with one AHU (Fig. 13).

The local DDC control demands can be conveniently collected by the supervisory controller when the AHU and VAV control stations are integrated in a single network. The static pressure is adjusted just allowing that the VAV dampers with the highest relative cooling load among all the VAV terminals is controlled to be very close to fully open position any time, in order to ensure that all the individual zones are supplied with sufficient air and the static pressure is controlled at its lowest allowed level.

When a large amount of VAV terminals are associated with one AHU, certain limited numbers of VAV dampers may be allowed to be fully open (or over the threshold) by setting the parameter (N_{\max}). Therefore, the first N_{\max} largest damper positions are neglected and the ($N_{\max} + 1$)st is used as the maximum control damper position by the controller actually. When the maximum damper position is over a threshold, which is set as the set-point of the PID, one PID function is activated to increase the static pressure set-point. On the contrary, the other PID function is activated to reduce the static pressure set-point when the maximum damper position is below the threshold. A hysteresis is added to the threshold as a 'dead band' of PID set-points to increase the stability of the control strategy. The static pressure set-point is determined by re-scaling the difference between the outputs of two PID functions within a pre-set pressure range.

5.4. AHU supply air temperature set-point reset

The air flow rate to a zone is reduced by closing down the VAV dampers when the load of a zone is low. Under low partial load, the total ventilation flow rate of a zone may be reduced to be very low in order to meet the reduced load. The reduction in total ventilation flow rate results in significant saving on fan power. On the other hand, a low ventilation flow rate may cause deficiencies of system performance, e.g. poor mixing of supply air and room air, inadequate room ambient air circulation and dumping [22]. When a minimum limit of the total ventilation flow rate is used, a space may be overcooled under low partial load if the supply air temperature is low.

The proper resetting of the supply air temperature allows the VAV system avoid the poor ventilation and save as much fan power as possible. A strategy for on-line reset of the supply air temperature set-point is illustrated in Fig. 14. The strategy utilises the air flow rate set-points of the pressure independent VAV damper controllers as the cooling load indicators of individual zones. The minimum flow set-point is set to avoid performance deficiency in individual zones, which may have different values for different zones and needs to be selected and tuned according to actual design and situation of individual zones. The upper flow rate set-point is a parameter used only for calculating the relative load of a zone. Since different zones may have very different flow ranges, the rate of the flow set-point of each zone is normalised using the ratios of the set-point to the minimum flow set-point and upper flow set-point, respectively.

The maximum ratio to upper flow set-point among zones is selected as the indicator of the relative load of zone with most critical thermal load. The minimum ratio to minimum flow set-point among zones indicates most critical zone in terms of ventilation. A positive value of

L_{PID} indicates that flow in certain zone is too low and the supply air temperature set-point needs to be increased. A large value of H_{PID} indicates that the load of a certain zone is high and the supply air temperature set-point needs to be reduced. The outputs of the PID functions are re-scaled within a pre-set range to determine the temperature set-point. The change rate limit is applied to the temperature set-point to ensure the stability of system control.

6. System simulation and test conditions

TRNSYS (A Transient System Simulation Program [5], developed in University of Wisconsin-Madison) is used as the platform for the dynamic simulation of the air-conditioning system including building zones and EMCS. Figure 15 shows a schematic of the major inter-connection between the component models (information flow diagram) for the system simulation. The component integration for pressure-flow balance, thermal balance, moisture and pollutant balance computation as well as for the temperature control, pressure control, flow control and supervisory control are illustrated.

The occupancy, lighting and equipment loads in each zone, the solar gain of each zone transmitted through the windows, 'sol-air' temperature of each zone, the outdoor air temperature, humidity and CO_2 concentration are provided by data files during simulation as test conditions. The transmission solar gain and equivalent 'sol-air' temperature are computed by a pre-processor prior to simulation according to building construction data, the solar radiation and outdoor air temperature recorded in the selected days.

The overall pollutant generation rate in the space is selected to be $1.0 * 10^{-6} \text{ m}^3/\text{s}$. The CO_2 , moisture and sensible heat generation rates of an occupant are selected to be $5 * 10^{-6} \text{ m}^3/\text{s}$, $1.17 * 10^{-5} \text{ kg/s}$ and 0.065 kW , respectively. The outdoor air CO_2 concentration is selected to be 360ppm as a constant. The internal load and occupancy profiles in the zones remained the same for the strategy evaluation exercises in different seasons. The air-conditioning system worked between 7:50 AM and 20:00 PM in the tests.

Figure 16 presents the overall lighting and equipment, sensible occupancy heat load, and number of occupants used in the simulation tests. The number of people varies significantly to introduce dynamic load to the cooling and ventilation system. Some occupants leave the office during lunch hour. The variation of lighting and equipment loads in the normal office hours represent the change of equipment load. The load reduces significantly in the late afternoon since occupants are leaving and therefore the lighting and equipment are switched off gradually.

Figure 17 shows the outdoor air dry bulb temperatures

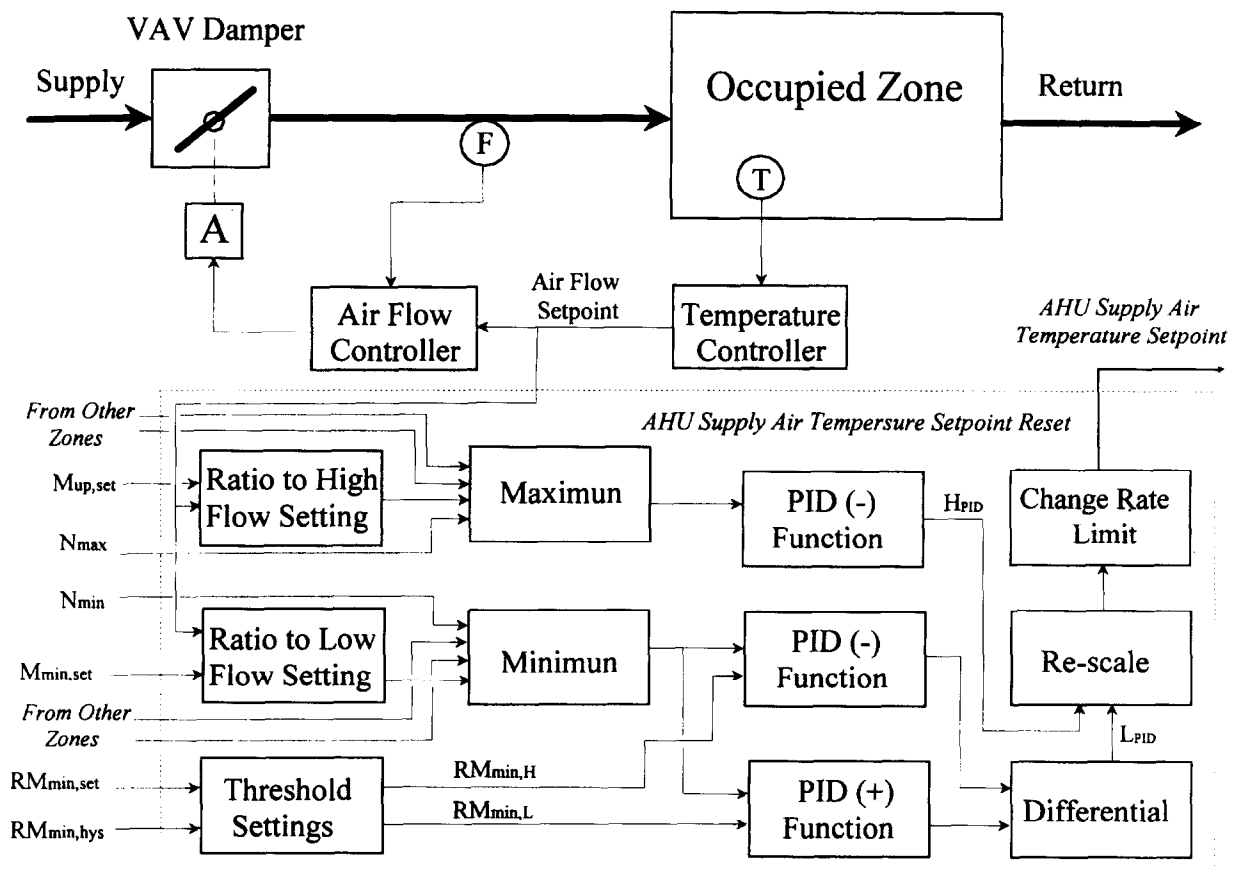


Fig. 14. Schematic of AHU outlet air temperature set-point supervisory strategy.

in four selected days. The four test cases are one sunny day in summer, one mild cloudy day in summer, one sunny day in spring and one sunny day in winter. The air temperature on the sunny day in summer varies between 26.7 and 33.4 °C while it varies between 29.1 and 33.4 °C during office hours (8:00–16:00). The air temperature on the mild cloudy day in summer varies between 27.6 and 29.7 °C during office hours. The air temperature on the sunny day in spring varies between 18.7 and 25 °C during office hours. The air temperature on the sunny day in winter varies between 14.2 and 15.7 °C during office hours.

Figure 18 shows the humidity of the outdoor air on the same days. The humidity on the spring day during office hours changes the most among the others. On the spring day the temperature and humidity in the afternoon increase significantly.

Figure 19 shows the overall solar heat gain of the perimeter zones transmitted through windows. The overall solar gain on the sunny summer case is the highest followed by the sunny spring case, the cloudy summer case and the sunny winter case. The period of solar radiation in the winter period is significantly shorter than that in other cases

7. Tests and evaluation of on-line control strategies

Two simulation exercises were conducted to test the dynamic response of DDC local control loops and evaluate the supervisory control strategies. In the first exercise, tests were carried out to tune the control loop, to commissioning the strategy programs and to check the capability of the system simulation package in evaluating the on-line control performance of temperature, pressure and flow control loops as well as the dynamic occupancy detection strategy. The second exercise was conducted to evaluate the dynamic response, the energy and environmental performances of pressure, temperature and fresh air set-point optimisation strategies.

Figure 20 shows some examples of controlled variables in the spring test case when the control loops were badly tuned. When improper PID parameters were used in the AHU VAV coil outlet air temperature control loop, the VAV fan control loop and fresh air control loop, respectively, strong oscillations occurred in those control loops. Figure 21 shows the same variables tested at same conditions after well tuning those control loops. The temperature, pressure and flow rate control loops were stabilised.

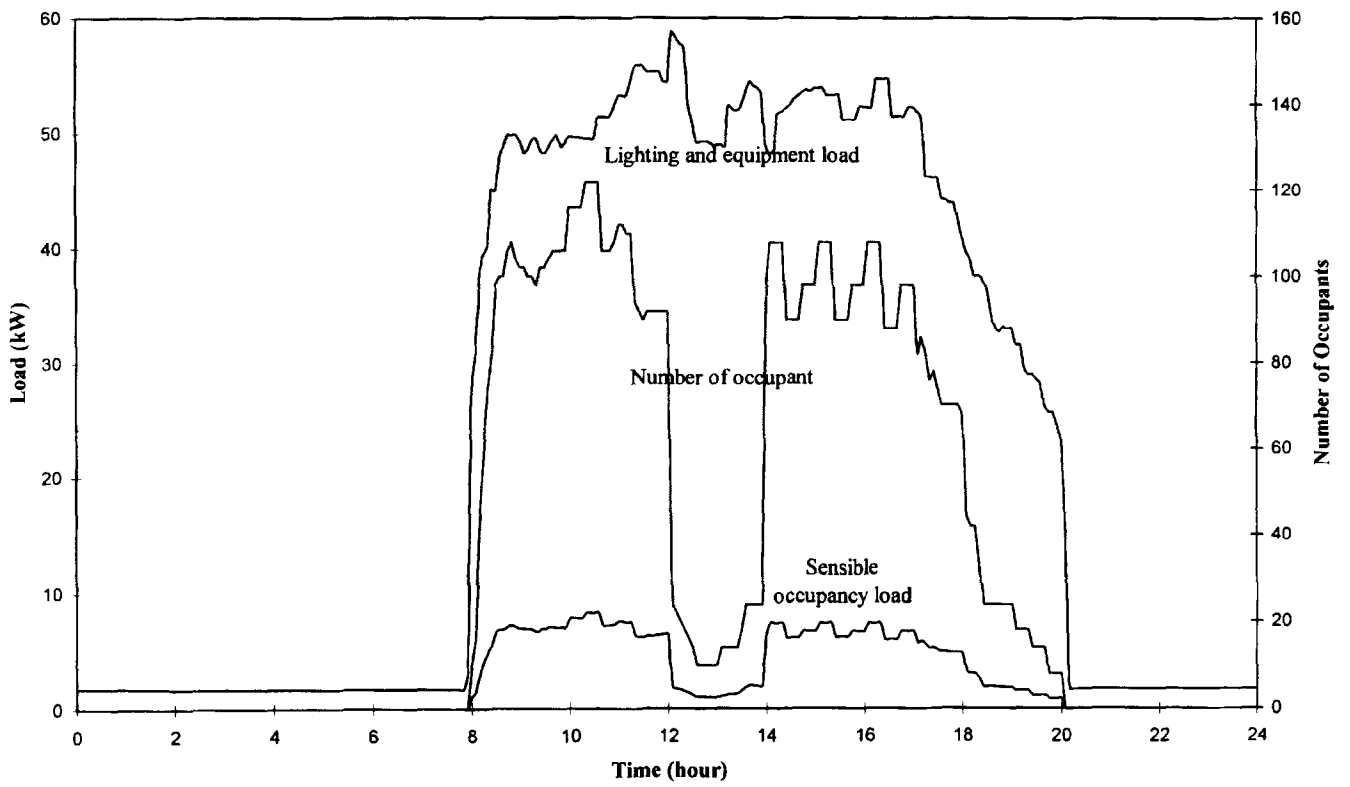


Fig. 16. Overall lighting, equipment and occupancy profiles.

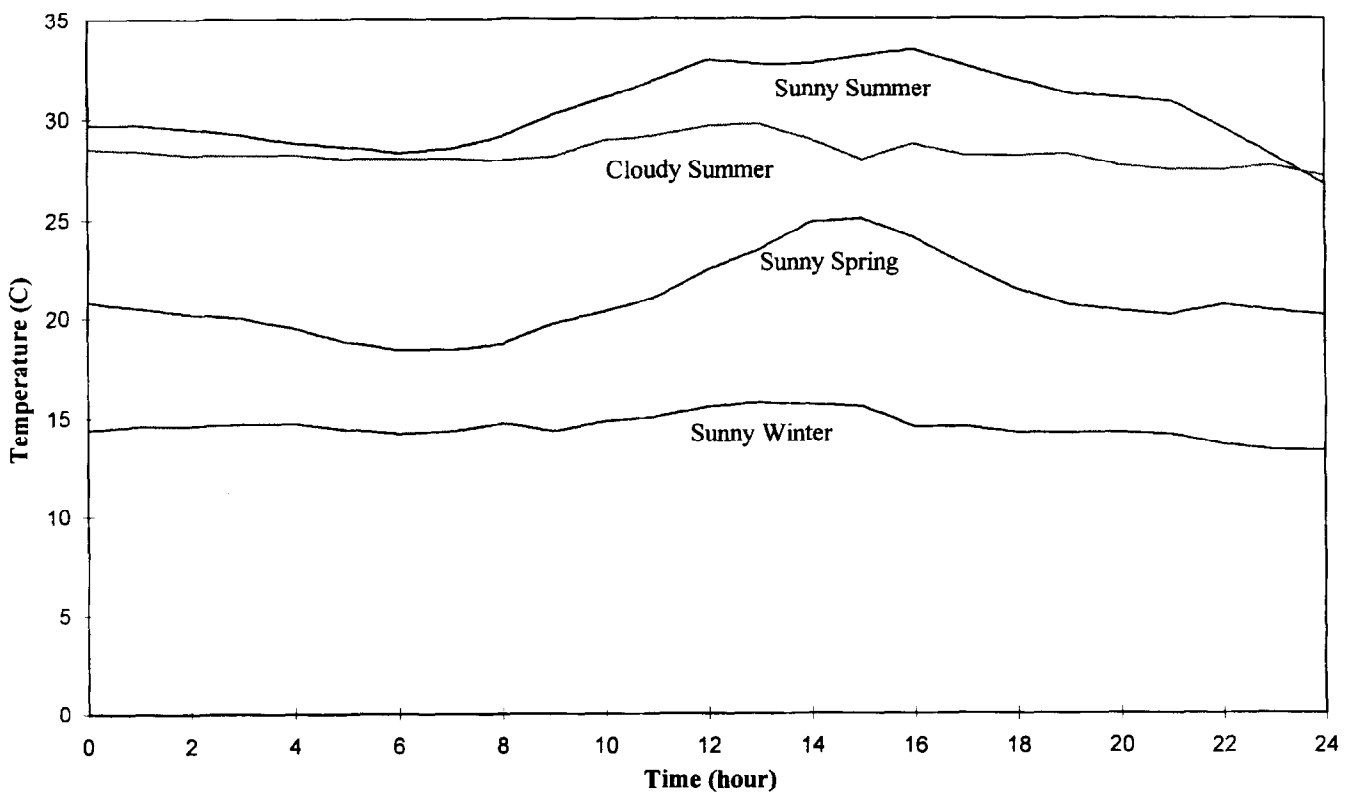


Fig. 17. Outdoor air dry bulb temperature on selected test days.

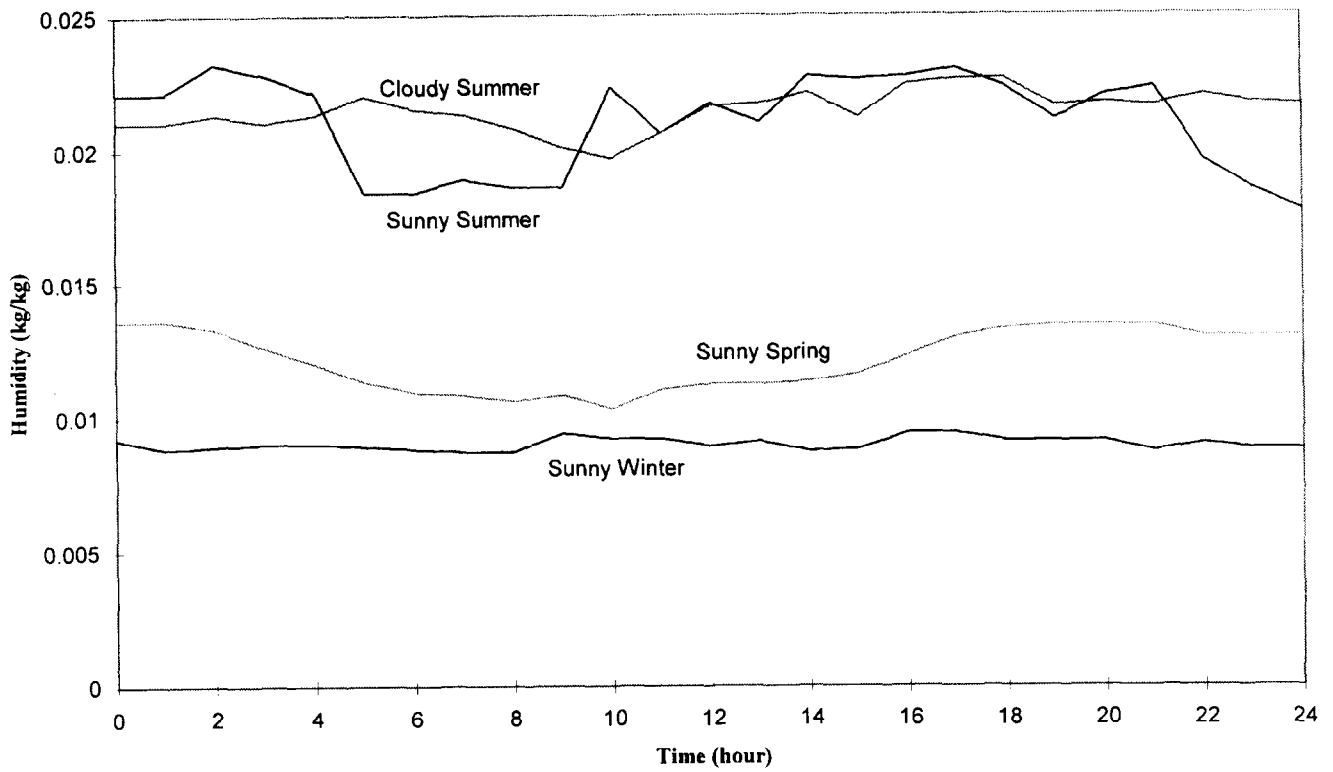


Fig. 18. Outdoor air humidity on selected test days.

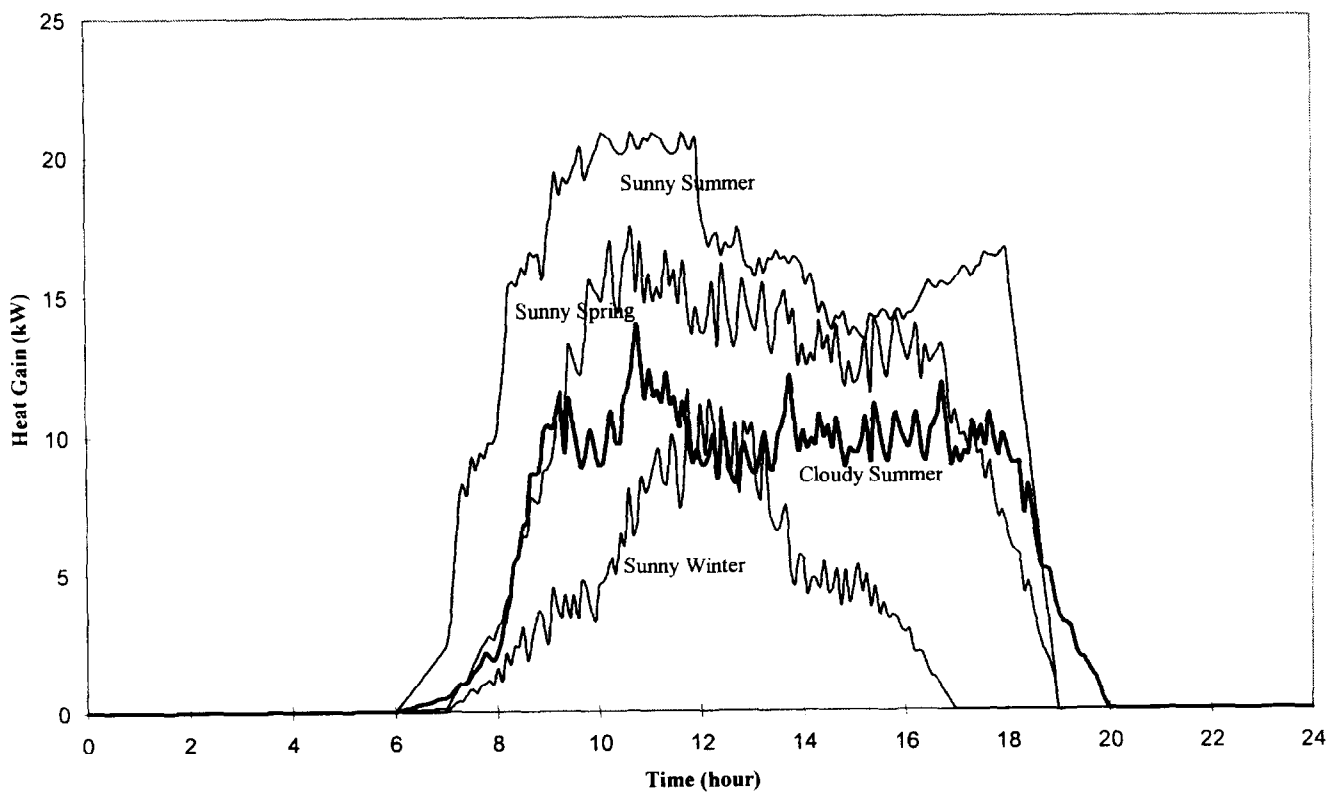


Fig. 19. Overall heat gain transmitted into perimeter zones on selected test days.

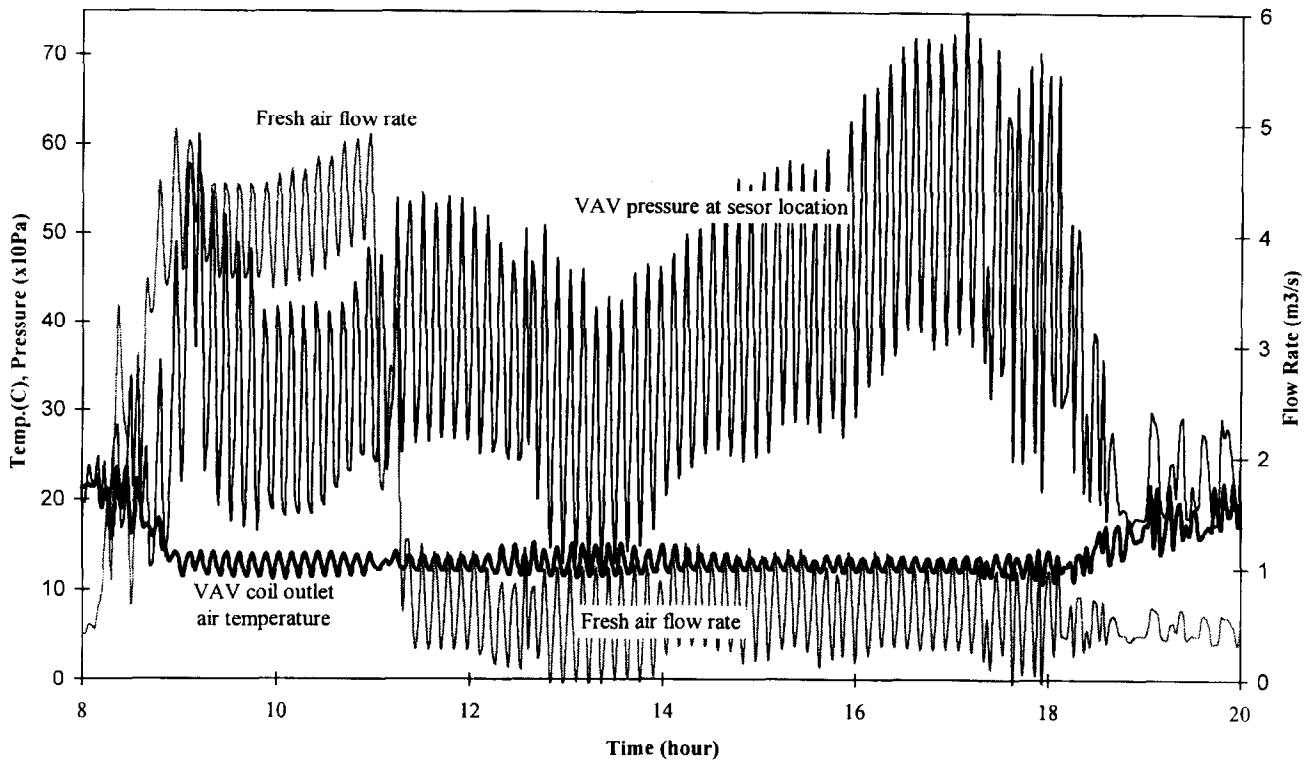


Fig. 20. Examples of controlled variables in badly tuned control loops.

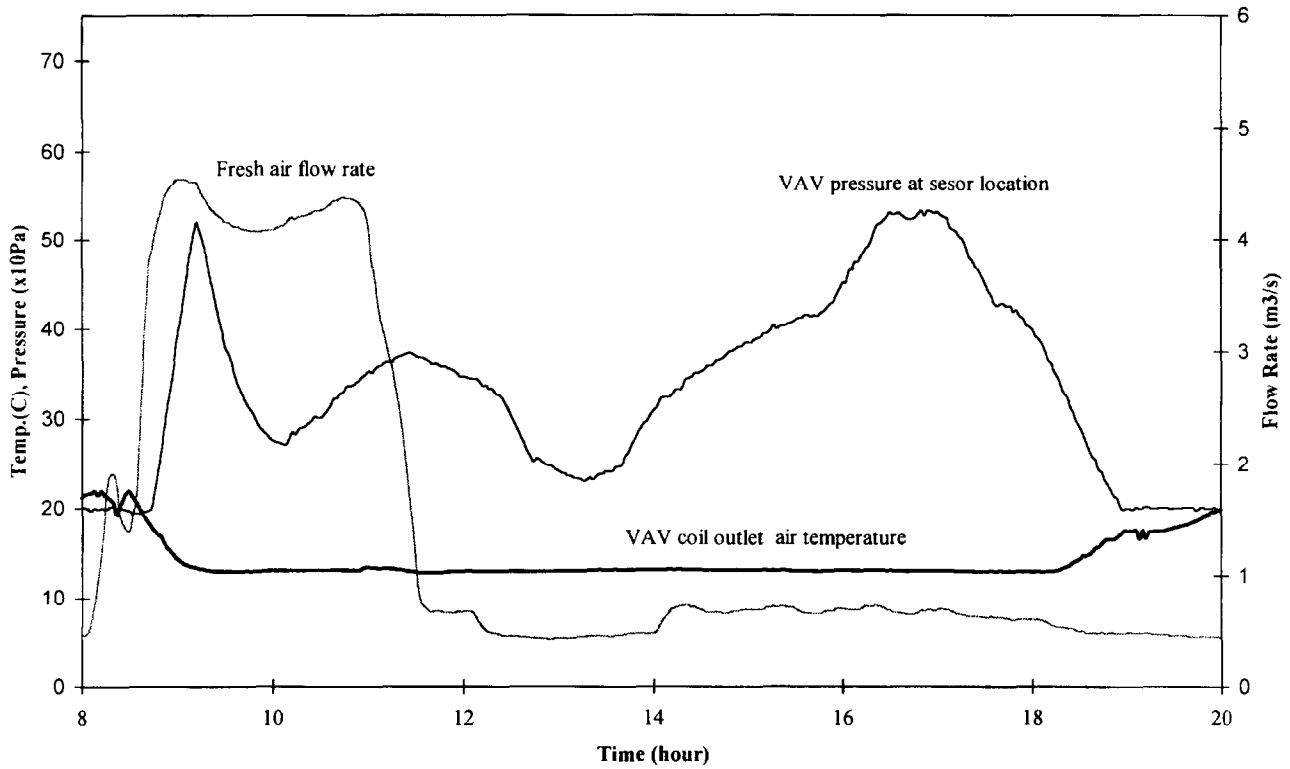


Fig. 21. Examples of controlled variables in well tuned control loops.

Figure 22 presents the occupancies detected by the occupancy detector when the fresh air flow was constant and when the flow air varied, respectively, as shown in Fig. 21. Different between the occupancies detected in two difference cases and between the detected and real occupancies can be observed. But only small differences were found between the detected and real occupancy, which will not affect the DVC to set a proper fresh air flow set-point.

In Exercise 2, five tests with different control strategies are conducted in each test day. These strategies are: 'Conventional'—constant set-points (i.e. 650 Pa for VAV static pressure, 14°C for AHU air temperature in the winter case and 13°C for other cases, 0.8 m³/s for outdoor air flow), 'AHU Temperature Optimisation'—only supervisory control for AHU temperature set-point is used, 'VAV Pressure Optimisation'—only supervisory control for VAV pressure set-point is used, 'Outdoor Air Flow Optimisation'—only supervisory control for outdoor air flow set-point is used. 'Overall Control Optimisation'—three supervisory control strategies are used together. The overall energy, comfort and environmental performance data using these strategies in four test days are presented in Tables 1-4. An overall COP of chilling system is assumed to be 2.5 as a constant when calculating the overall electricity use.

Figure 23 shows the VAV static pressure set-point of

the system in the four different test days when the static pressure supervisory control was employed. In both summer days, the pressure was set at its maximum when the system was turned on, since the temperature in the occupied zones were high. It was set at minimum in the other two test days since the initial room temperature is low. The peaks in the morning and in the afternoon were due to the high solar gains to the perimeter zones facing east and west, respectively. The valley in the lunch hours was due to two reasons: the reduction of occupancy load, and even distribution and reduction of solar gains to the perimeter zones. In the late afternoon, the set-point was set at minimum due to the reduction of the internal and external loads. In overall, the level of pressure set-point had no significant difference between three test days since the summer day is cloudy and the CAV system in the winter day was turned off.

Compared with the 'Conventional' control strategy, the total fan electricity consumption was reduced by 2.87, 8.52, 9.25 and 15.01% in the four test days, respectively. That indicates that more saving in the fan consumption can be achieved by using VAV static pressure reset when the weather is cold and when there is no high solar heat gain. Saving in fan consumption can be achieved even in sunny summer since the system might not always work in full load the whole day. The test also shows that the use of pressure set-point optimisation did not affect the

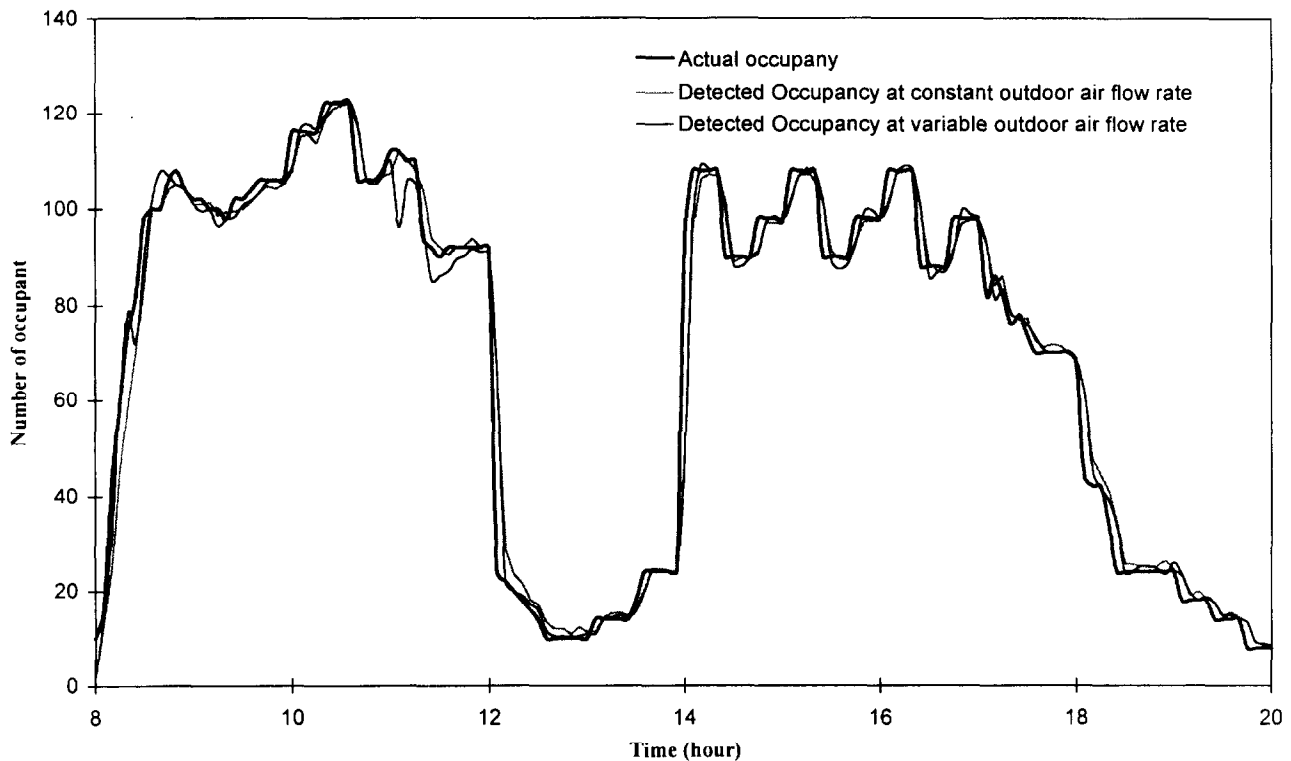


Fig. 22. Comparison between actual occupancy and detected occupancies in two different cases.

Table 1
Summary of energy and environment data of tests in sunny summer case

Strategy	Conventional	AHU temp optimization	VAV pressure optimization	Outdoor air flow optimization	Overall control optimization
VAV fan consumption (MJ)	524.49	521.95	493.89	513.5	480.08
CAV fan consumption (MJ)	159.83	159.83	159.83	159.83	159.83
Return fan consumption (MJ)	435.70	433.73	434.10	423.28	420.09
Total fan consumption (MJ)	1120.02	1115.51	1087.82	1096.61	1060.00
<i>Saving (%)</i>	—	0.40	2.87	2.09	5.36
VAV coil consumption (MJ)	3826.29	3782.69	3823.69	3534.16	3489.71
CAV coil consumption (MJ)	1268.92	1251.52	1270.64	1192.6	1173.60
Total coil consumption (MJ)	5095.21	5034.21	5094.33	4726.76	4663.31
<i>Saving (%)</i>	—	1.20	0.02	7.23	8.48
Overall electricity use (MJ)	3158.10	3129.19	3125.55	2987.31	2925.32
<i>Saving (%)</i>	—	0.92	1.03	5.41	7.37
Average CO ₂ (ppm)	810.1	810.0	810.1	912.5	912.7
<i>Maximum CO₂ (ppm)</i>	<i>987.4</i>	<i>987.6</i>	<i>987.5</i>	<i>1039.0</i>	<i>1039.0</i>
Average pollutant (ppm)	1.38	1.38	1.38	1.75	1.75
<i>Maximum pollutant (ppm)</i>	<i>3.53</i>	<i>3.53</i>	<i>3.52</i>	<i>4.01</i>	<i>4.03</i>
Average PPD (%)	5.23	5.22	5.23	5.24	5.22
<i>Maximum PPD (%)</i>	<i>5.95</i>	<i>5.56</i>	<i>5.93</i>	<i>6.14</i>	<i>5.55</i>

Table 2
Summary of energy and environment data of test in cloudy summer case

Strategy	Conventional	AHU temp. optimization	VAV pressure optimization	Outdoor air flow optimization	Overall control optimization
VAV fan consumption (MJ)	404.43	402.64	332.83	397.06	324.5
CAV fan consumption (MJ)	159.83	159.83	159.83	159.83	159.83
Return fan consumption (MJ)	310.62	310.05	307.68	302.59	299.21
Total fan consumption (MJ)	874.88	872.52	800.34	859.48	783.54
<i>Saving (%)</i>	—	0.27	8.52	1.76	10.44
VAV coil consumption (MJ)	3149.91	3100.98	3148.87	2903.51	2854.41
CAV coil consumption (MJ)	1302.97	1280.27	1303.68	1223.91	1198.77
Total coil consumption (MJ)	4452.88	4381.25	4452.55	4127.42	4053.18
<i>Saving (%)</i>	—	1.61	0.01	7.31	8.98
Overall electricity use (MJ)	2656.03	2625.02	2581.36	2510.45	2404.81
<i>Saving (%)</i>	—	1.17	2.81	5.48	9.46
Average CO ₂ (ppm)	809.1	809.0	809.1	906.8	906.8
<i>Maximum CO₂ (ppm)</i>	<i>986.7</i>	<i>986.1</i>	<i>986.4</i>	<i>103.4</i>	<i>1033.0</i>
Average pollutant (ppm)	1.37	1.37	1.37	1.73	1.74
<i>Maximum pollutant (ppm)</i>	<i>3.53</i>	<i>3.52</i>	<i>3.54</i>	<i>4.07</i>	<i>4.11</i>
Average PPD (%)	5.27	5.24	5.27	5.28	5.23
<i>Maximum PPD (%)</i>	<i>6.55</i>	<i>5.44</i>	<i>6.52</i>	<i>6.74</i>	<i>5.46</i>

cooling coil consumption, the thermal comfort and environmental performance indicating that the supply air flow and distribution was not affected.

Figure 24 shows the outdoor air flow rate set-point of the system in the four different test days when the outdoor air flow supervisory control was employed. During the whole day in the winter case and some period of spring case, 100% of outdoor air was set since the outdoor enthalpy is lower than that of the return air (however, the outdoor air used actually was less than 100% even when the fresh air damper was set at maximum open position and the recycle air damper was set at closed

position due to the significant leakage of the recycle air damper introduced in the system). In the other cases, the outdoor air flow rate was at its minimum demanded level set by the demanded ventilation control according to the detected occupancy.

Compared with the 'Conventional' control strategy, the total cooling coil consumption was reduced by 7.23, 7.31, 1.57 and 78.76% in the four test days, respectively. That indicates the significant reduction on cooling coil consumption can be achieved either by demanded ventilation control when outdoor air enthalpy is relatively high or by free (partially free) cooling when the outdoor

Table 3
Summary of energy and environment data of tests in sunny spring case

Strategy	Conventional	AHU temp. optimization	VAV pressure optimization	Outdoor air flow optimization	Overall control optimization
VAV fan consumption (MJ)	336.62	348.94	268.17	334.65	285.24
CAV fan consumption (MJ)	159.83	159.83	159.83	159.83	159.83
Return fan consumption (MJ)	249.32	265.9	248.78	249.67	266.98
Total fan consumption (MJ)	745.77	774.67	676.78	744.15	712.05
<i>Saving (%)</i>	—	−3.88	9.25	0.22	4.52
VAV coil consumption (MJ)	1858.10	1789.59	1855.66	1811.05	1721.44
CAV coil consumption (MJ)	892.56	785.51	893.21	896.5	759.47
Total coil consumption (MJ)	2750.66	2575.10	2748.87	2707.55	2480.91
<i>Saving (%)</i>	—	6.38	0.07	1.57	9.81
Overall electricity use (MJ)	1846.03	1804.71	1776.33	1827.17	1704.41
<i>Saving (%)</i>	—	2.24	3.78	1.02	7.67
Average CO ₂ (ppm)	809.9	809.1	809.9	739.9	726.5
<i>Maximum CO₂ (ppm)</i>	996.5	986.5	986.9	997.1	996.8
Average pollutant (ppm)	1.38	1.38	1.38	1.12	1.00
<i>Maximum pollutant (ppm)</i>	3.63	3.62	3.63	4.32	2.98
Average PPD (%)	5.70	5.33	5.69	5.72	5.34
<i>Maximum PPD (%)</i>	10.78	6.61	10.73	11.03	6.88

Table 4
Summary of energy and environment data of tests in sunny winter case

Strategy	Conventional	AHU Temp. optimization	VAV Pressure optimization	Outdoor air flow optimization	Overall control optimization
VAV fan consumption (MJ)	354.42	399.87	276.33	351.77	315.45
CAV fan consumption (MJ)	0.00	0.00	0.00	0.00	0.00
Return fan consumption (MJ)	166.15	182.35	166.11	168.71	176.73
Total fan consumption (MJ)	520.57	582.22	442.44	520.48	492.18
<i>Saving (%)</i>	—	−11.84	15.01	0.02	5.45
VAV coil consumption (MJ)	1173.71	1102.20	1171.36	249.31	304.57
CAV coil consumption (MJ)	0.00	0.00	0.00	0.00	0.00
Total coil consumption (MJ)	1173.71	1102.20	1171.36	249.31	304.57
<i>Saving (%)</i>	—	6.09	0.20	78.76	74.05
Overall electricity use (MJ)	990.05	1023.10	910.98	620.20	614.08
<i>Saving (%)</i>	—	−3.34	7.99	37.36	37.98
Average CO ₂ (ppm)	775.6	797.1	774.7	484.6	509.0
<i>Maximum CO₂ (ppm)</i>	936.0	973.9	936.0	613.0	795.8
Average pollutant (ppm)	1.13	1.20	1.12	0.33	0.58
<i>Maximum pollutant (ppm)</i>	2.88	2.88	2.77	1.34	3.36
Average PPD (%)	5.78	5.51	5.77	5.74	5.41
<i>Maximum PPD (%)</i>	13.33	9.28	13.20	13.45	8.84

air enthalpy is relatively low. The reduction on coil consumption is not significant when the outdoor enthalpy is close to that of the return air. The demanded ventilation control can control the pollutant and CO₂ within the allowed level whilst the use of more outdoor air will reduce the indoor air pollutant and CO₂ level. Resetting the outdoor air flow does not affect the indoor thermal comfort control.

Figure 25 shows the AHU outlet air temperature set-point in the four different test days when AHU air temperature supervisory control was used. Both in the winter and spring cases, the temperature set-point was set at its

maximum since the low initial indoor air temperature as well as the low cooling load in the winter case. In all the four cases, the temperature set-point was increased in the late afternoon since the load is very low. It was observed that the problem of insufficient total ventilation was overcome by resetting the temperature set-point, which occurred in certain zones when the AHU temperature set-point was set at a low constant point. The fan consumption was increased significantly in winter case and spring case (11.84 and 3.88%, respectively) since more total ventilation flow was used to avoid insufficient air flow as shown in Fig. 26. The cooling coil consumption

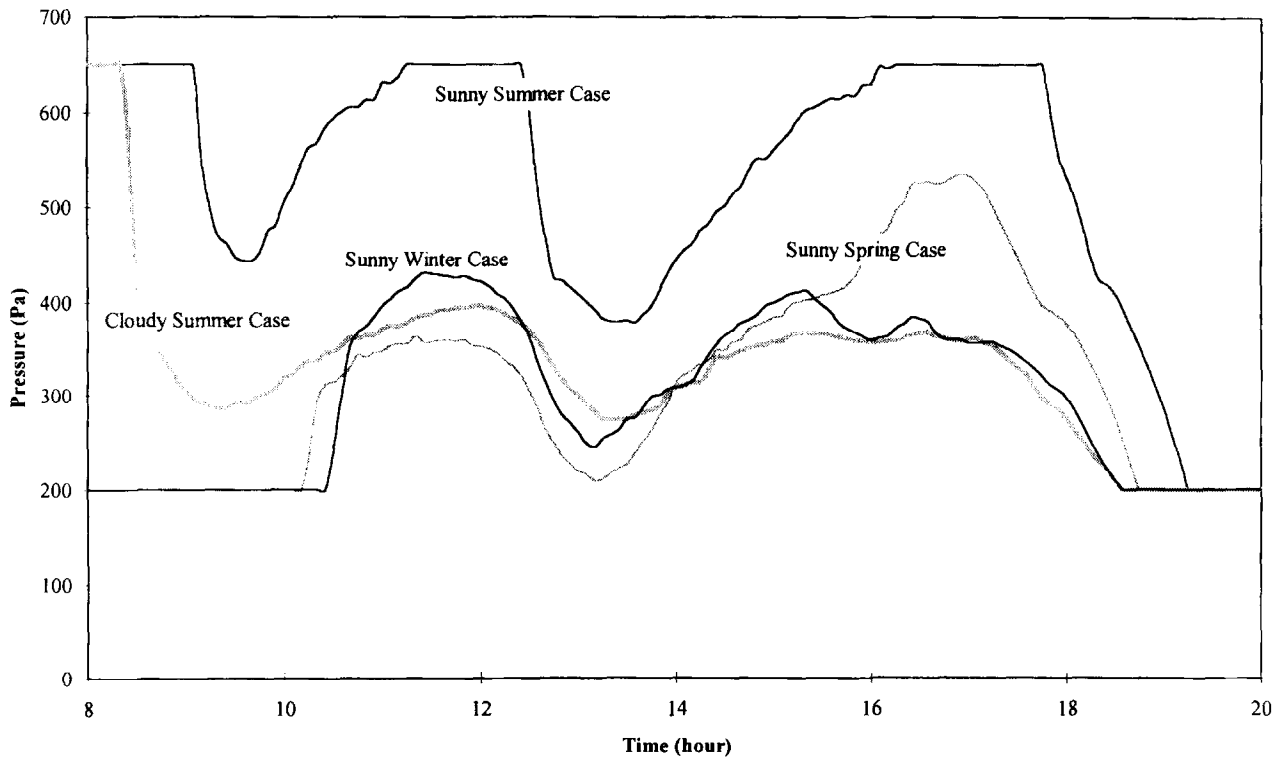


Fig. 23. VAV static pressure set-point using pressure set-point reset strategy in four seasons.

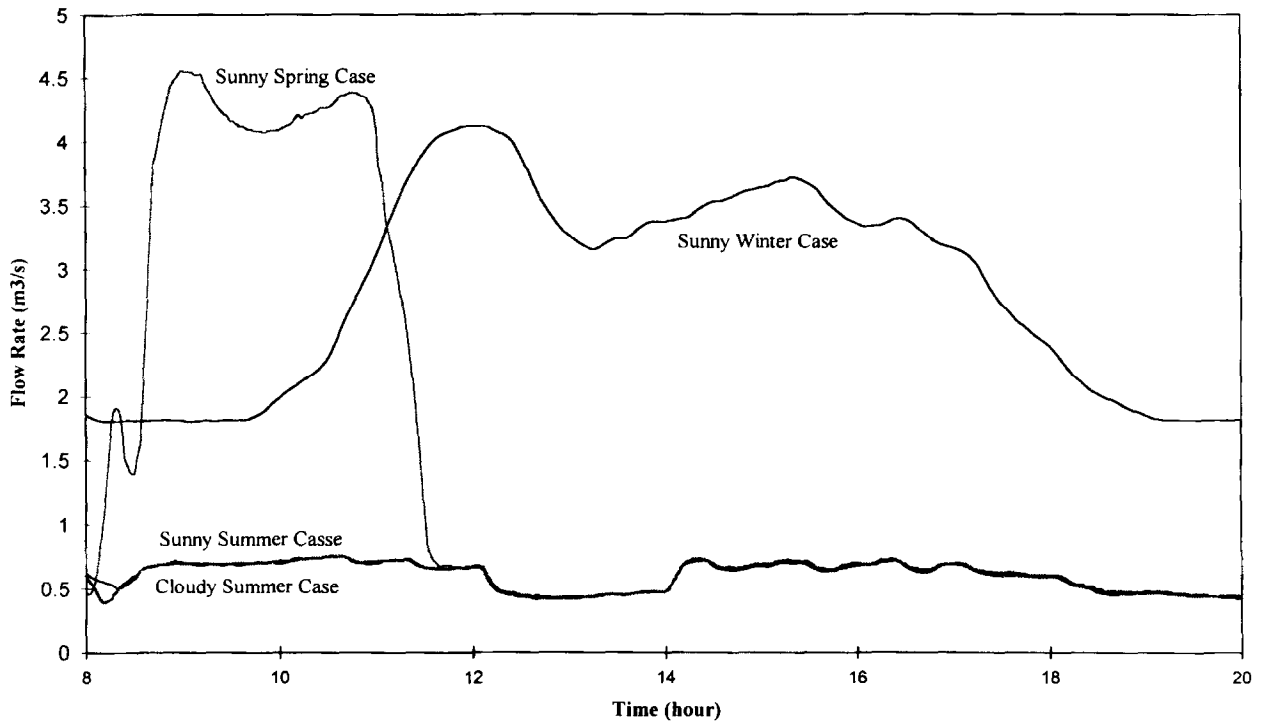


Fig. 24. Outdoor ventilation air flow rate set-point using flow rate set-point strategy in four seasons.

in these two test cases was significantly reduced (6.09 and 6.38%, respectively) since the overcooling in many zones was avoided as indicated by the improvement of the

thermal comfort when resetting the AHU temperature set-point.

When optimising the AHU air temperature set-point,

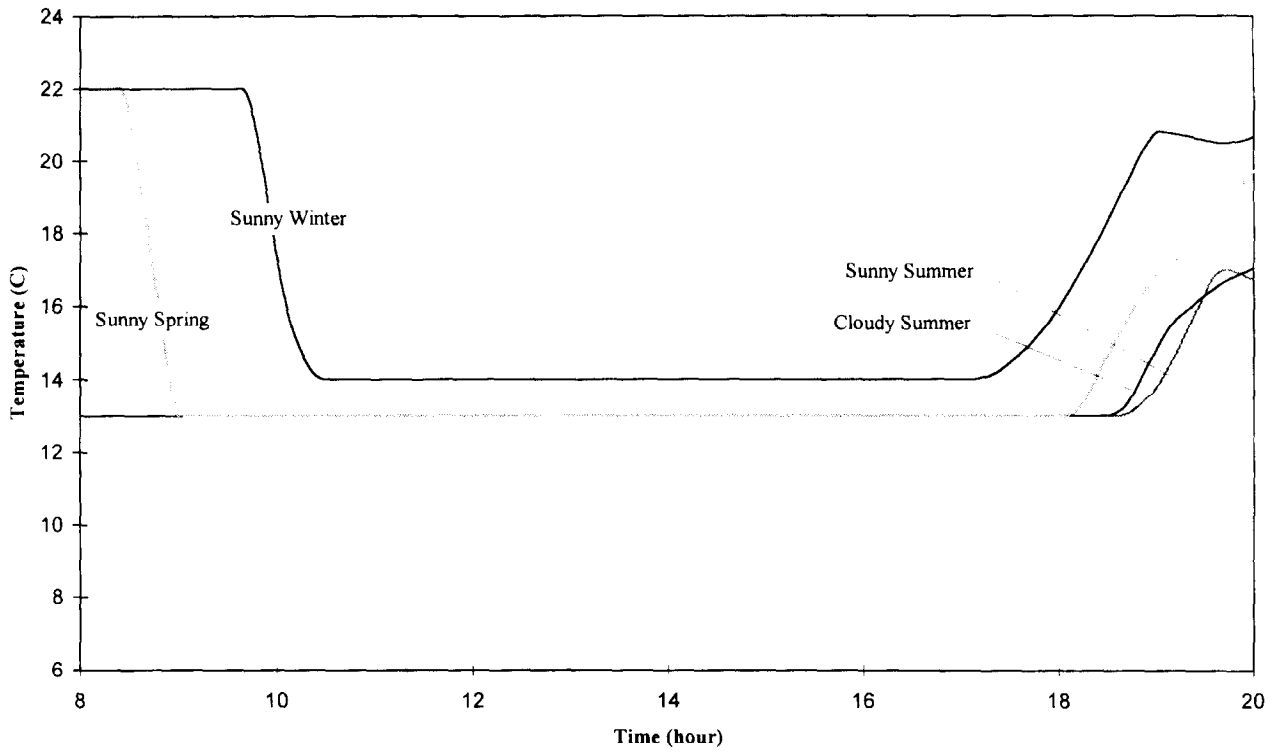


Fig. 25. AHU outlet air temperature using temperature set-point reset strategy in four seasons.

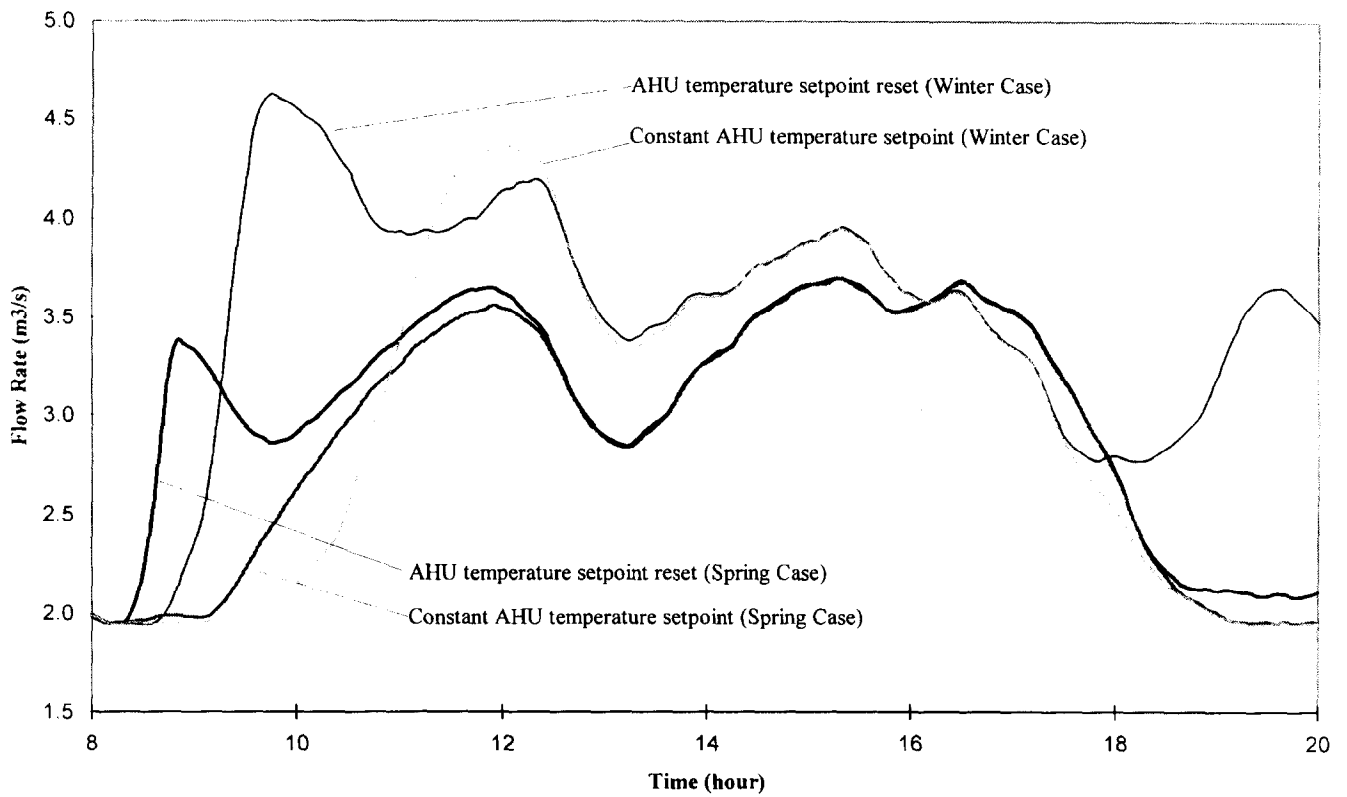


Fig. 26. Comparison between the total VAV ventilation flows using constant AHU temperature and AHU temperature reset strategies in winter and spring test cases.

the VAV static pressure set-point and outdoor air flow set-point at the same time, both the fan consumption and cooling coil consumption were reduced significantly. The saving in HVAC electricity consumption by employing the three supervisory strategies was 7.37, 9.46, 7.67 and 37.98% in the sunny summer, cloudy summer, spring and winter test cases, respectively. The indoor thermal comfort was improved in all the test cases. The CO₂ and pollutant level was reduced in the winter and spring cases whilst sufficient outdoor ventilation air was provided in the summer test cases.

8. Summary and conclusions

Simulation tests show that dynamic simulation is a convenient and suitable tool in testing and evaluating the dynamic, environmental and energy performances of air-conditioning systems and their on-line control strategies. The control strategies can be tested and evaluated on 'living systems' with very limited cost and time using computer simulation. The control software packages can be tested and commissioned under realistic environments prior to the implementation in real EMCS. The supervisory and local control strategies can also be pre-tuned before being utilised in real systems.

The thermal, hydraulic, environmental, mechanic dynamics characteristics and energy performance of the system can be simulated using the conventional component-based dynamic and energy performance simulation programs such as TRNSYS, that allows us make use of the available component models well validated. However, convergence when integrating all those characteristics in the programs might be a problem, which needs proper solutions in applications.

Evaluation tests also show that integrated digital controllers (EMCS) provide promising potentials in optimising the control and operation of VAV air-conditioning systems. Both significant saving in energy and improvement on indoor environment can be achieved by optimising the set-points of AHU supply air temperature, the outdoor ventilation air flow and the static pressure of VAV air-conditioning systems with at most no additional cost by utilising the integrated digital controllers which are often available in the newly designed office buildings.

Acknowledgements

The research work presented in the paper is financially supported by a University Research Grant. The author would also like to note the fruitful benefits from the collaboration and exchange among the participants of

IEA joint project Annex 30 (Bringing Simulation into Application) when conducting the research work.

References

- [1] Lebrun J, Wang SW. Evaluation and Emulation of Building Energy Management Systems—Synthesis Report, IEA (BCS) Annex 17 Final Report, University of Liege, Belgium, 1993.
- [2] Wang SW. Dynamic simulation of a building central chilling system and evaluation of EMCS on-line control strategies. *Building and Environment* 1997; 32(2).
- [3] Zaheer-Uddin M, Zheng GR. A dynamic model of multizone VAV system for control analysis. *ASHRAE Transaction* 1994; 100(1).
- [4] House JM. A system approach to optimal control for HVAC and building systems. *ASHRAE Transaction* 1995; 101(2).
- [5] Klein SA et al. TRNSYS—A Transient Simulation Program, User Manual version 13.1, 1990.
- [6] LBL DOE-2 Engineering Manual version 2.1c. Berkeley, CA, Lawrence Berkeley Laboratory, 1982.
- [7] Park C, Clark DR, Kelly GE. HCACSIM+ Building Systems and Equipment Simulation Program: Building Loads Calculation. National Institute of Standards and Technology, Gaithersburg, 1986.
- [8] Emmerich SJ, Mitchell JW, Beckman WA. Demand-controlled ventilation in a multi-zone office building. *Indoor environment* 1994; 3:331–40.
- [9] ASHRAE: ASHRAE Standard 62-1989R, Ventilation for Acceptable Indoor Quality (Public Review Draft). ASHRAE, August, 1996.
- [10] Laret L, Liebecq G, Ngendakumana P. Building. IEA Annex 10 Report, University of Liege, Belgium, 1987.
- [11] Wang SW. Modelling and simulation of Building and HVAC System—Building and HVAC Component Models Used in Simulation Exercise C.3. IEA Annex 17 Report, University of Liege, Belgium, 1992.
- [12] Skistad H. Displacement Ventilation. Research Studies Press Ltd., England, 1994.
- [13] Holmes M. Room Air Movement with Ceiling Mounted Diffusers. *BSRIA*, 2/75.
- [14] Schlichting H. *Boundary-Layer Theory*. McGraw-Hill, New York, 1979.
- [15] Legg RC. Characteristics of single and multi-blade dampers for duct air systems. *Building Services Engineering and Technology* 1987; 7(8).
- [16] Crrado V, Mazza A. Axial Fan. IEA Annex 17 Report, Politecnico di Torino, Italy, 1991.
- [17] Lebrun J, Ding X, Eppe JP, Wasacz. Cooling coil models to be used in transient and/or wet regimes—theoretical analysis and experimental validation. *Proceedings of System Simulation in Buildings 1990*, Liege, Belgium, 1990.
- [18] Wang SW, Burnett J. BEMS control strategies: Evaluation of realistic performance by computer simulation. *Building Services Engineering Research and Technology* 1996; 17(1).
- [19] Haves P, Dexter AL. Simulation of local loop controls. *Proc. Building 1989*, IBPSA, Vancouver, 1989.
- [20] Janu GJ, Wenger JD, Nesler CG. Outdoor Air Flow Control for VAV Systems. *ASHRAE Journal*, April, 1995.
- [21] Englander SL, Norford LK. Saving Fan Energy in VAV Systems—Part 2: Supply Fan Control for Static Pressure Minimisation Using DDC Zone Feedback. *ASHRAE Transactions* 100, 1993.
- [22] Coad W. Indoor Air Quality: A Design Parameter. *ASHRAE Journal*, June, 1996.